

A ROBUST MEASURE OF TIDAL CIRCULARIZATION IN COEVAL BINARY POPULATIONS: THE SOLAR-TYPE SPECTROSCOPIC BINARY POPULATION IN THE OPEN CLUSTER M35 ¹

Søren Meibom^{2,4} and Robert D. Mathieu^{3,4}

Astronomy Department, University of Wisconsin - Madison, Madison, WI - 53706, USA

ABSTRACT

We present a new homogeneous sample of 32 spectroscopic binary orbits in the young (~ 150 Myr) main-sequence open cluster M35. The distribution of orbital eccentricity vs. orbital period ($e - \log(P)$) displays a distinct transition from eccentric to circular orbits at an orbital period of ~ 10 days. The transition is due to tidal circularization of the closest binaries. The population of binary orbits in M35 provide a significantly improved constraint on the rate of tidal circularization at an age of 150 Myr. We propose a new and more robust diagnostic of the degree of tidal circularization in a binary population based on a functional fit to the $e - \log(P)$ distribution. We call this new measure the *tidal circularization period*. The tidal circularization period of a binary population represents the orbital period at which a binary orbit with the most frequent initial orbital eccentricity circularizes (defined as $e = 0.01$) at the age of the population. We determine the tidal circularization period for M35 as well as for 7 additional binary populations spanning ages from the pre main-sequence (~ 3 Myr) to late main-sequence (~ 10 Gyr), and use Monte Carlo error analysis to determine the uncertainties on the derived circularization periods. We conclude that current theories of tidal circularization cannot account for the distribution of tidal circularization periods with population age.

Subject headings: clusters: open, spectroscopic binaries, tidal circularization

¹WIYN Open Cluster Study. XXII.

²*meibom@astro.wisc.edu*

³*mathieu@astro.wisc.edu*

⁴Visiting Astronomer, Kitt Peak National Observatory, National Optical Astronomy Observatory, which is operated by the Association of Universities for Research in Astronomy, Inc. (AURA) under cooperative agreement with the National Science Foundation.

1. INTRODUCTION

In a coeval population of binary stars the closest binaries (separations $\lesssim 0.5$ AU) tend to have circular orbits, while wider binaries have orbits with a distribution of non-zero eccentricities. This trend holds true for binaries with early-type (North & Zahn 2003; Pan et al. 1998; Matthews & Mathieu 1992; Giuricin et al. 1984) as well as late-type (Mathieu et al. 2004; Latham et al. 2002; Melo et al. 2001; Mathieu et al. 1992) main-sequence components, for binaries with evolved stellar components (Mermilliod & Mayor 1992), and in the orbital eccentricity distribution of large planets around solar-type stars (<http://exoplanets.org>). The transition from eccentric to circular orbits is explained by dissipative tidal interactions caused by the reaction of the binary components to each other’s gravitational field (tidal circularization: Hut 1981; Zahn 1977; Darwin 1879). The theory of tidal interactions predicts that the timescale of circularization depends strongly on stellar separation. Consequently, for a coeval binary population, the transition from eccentric to circular orbits should occur at a well-defined binary period. However, despite the coeval nature of a star cluster, its population of short period binaries may be small in number and consist of systems with a distribution of initial eccentricities, masses, and stellar angular momenta. Accordingly, the size and heterogeneity of the binary population will add complexity and uncertainty to the observational determination of the tidal circularization period.

Nonetheless, the transition between eccentric and circular binary orbits provides an important constraint on the rate of tidal circularization as a function of orbital period, integrated over the lifetime of a binary population. Furthermore, the distribution of tidal circularization periods with population age enables us to study the evolution of tidal circularization with time.

The success of theoretical models describing the efficiency and the evolution of tidal circularization can be measured by their ability to “predict” the tidal circularization periods for binary populations of different ages. The differences between present-day models lie in the mechanism by which energy and angular momentum is transported between the binary components and their orbits. Currently, three theoretical models exist for the mechanism for tidal dissipation in late-type main-sequence stars: 1) *The equilibrium tide theory* describes retardation of the hydrostatic tidal bulge (equilibrium tide) due to the coupling of the tidal flow to the motion of turbulent eddies in the stellar convective envelope. This dissipative coupling is assumed to be responsible for a phase shift between the tidal bulge and the orbital motion of the binary stars. Because of the phase shifts a tidal torque is established between the two stars (Zahn 1977; Hut 1981); 2) *The theory of dynamical tides* describes the excitation and damping of gravity (g) waves in the radiative zones of stars due to the tidal forcing by the companion star (Savonije & Papaloizou 1983; Zahn 1977, 1975, 1970).

This dissipation mechanism has been successfully applied to explain circularization of early-type main-sequence stars with radiative envelopes (Claret & Cunha 1997; Giuricin et al. 1984; Zahn 1977), and recently has also been applied to the radiative cores of late-type stars (Savonije & Witte 2002; Witte & Savonije 2002; Goodman & Dickson 1998; Terquem et al. 1998). Inclusion of resonance locking between the tidally forced modes and stellar eigenmodes provides increased efficiency of the tidal coupling (Savonije & Witte 2002; Witte & Savonije 2002, 2001, 1999a,b); 3) A pure *hydrodynamical mechanism* has been proposed by Tassoul (2000, 1988) and Tassoul & Tassoul (1996). Tassoul suggests that hydrodynamical flows (large-scale meridional currents) induced by lack of symmetry about the rotation axis in the tidally perturbed star are responsible for the tidal torques on the component stars. This mechanism has been controversial on theoretical grounds (Rieutord 1992; Rieutord & Zahn 1997; Tassoul & Tassoul 1997).

Despite the developments in the theory of tidal circularization, the models still cannot account for the observed periods of circular orbits in solar-mass binary populations (e.g. Witte & Savonije 2002; Claret & Cunha 1997; Mathieu et al. 1992). To help along further progress of theoretical modeling there is a need for high quality observational data on large and coeval samples of binary stars, allowing for accurate determination of the transition from eccentric to circular orbits.

This paper presents a homogeneous ($M_{prim} \sim 1 M_{\odot}$) sample of 32 spectroscopic binary orbits in the open cluster M35 (NGC 2168; $\alpha_{2000} = 6^h 9^m$, $\delta_{2000} = 24^{\circ} 20'$; $l = 186.59^{\circ}$, $b = 2.19^{\circ}$, distance $\simeq 850 pc$). With an age similar to the Pleiades but approximately three times richer, M35 is a benchmark for stellar astrophysics at $\sim 150 Myr$ (Deliyannis et al. 2004, in preparation). The age makes M35 an important testing ground for binary stars that have recently ended their pre main-sequence (PMS) phase where they were larger and fully convective. Thus M35 sets the initial state for main-sequence tidal circularization.

Section 2 describes the observations, instrument, and telescope used in the spectroscopic survey of M35. In Section 3 we present the distribution of orbital eccentricity as a function of orbital period in M35 (the $e - \log(P)$ diagram). In Section 4 we motivate and present a new robust method for determining the period at which the most frequent binary orbits circularize. We will call this the *tidal circularization period*. In Section 5 we discuss and compare our new diagnostic to the previous measure of tidal circularization, the tidal circularization cutoff period. We compare the precision and accuracy performance of both diagnostics and determine measurement uncertainties on the tidal circularization period. In Section 6 we determine the tidal circularization period for the binary population in M35, and in Section 7 we determine the circularization period for a series of published populations of late-type unevolved main-sequence binaries. In Section 8 we carry out a comparison between

current theoretical predictions of the efficiency and evolution of tidal circularization and the circularization periods derived in Sections 6 and 7. Section 9 summarizes and presents our conclusions.

2. OBSERVATIONS

M35 has been included in the WIYN Open Cluster Study (WOCS) program since 1997. The radial-velocity survey of the cluster will be described in detail in Meibom et al. (in preparation). We summarize the relevant points here. The initial selection of ~ 2000 target stars was based on photometric membership in the cluster and proper-motion membership studies to $V \lesssim 15$ by McNamara & Sekiguchi (1986) and Cudworth (1971). Bjorkman & Mathieu (unpublished) completed astrometry and photometry to $V \sim 17$. Our radial-velocity study includes stars from $V \simeq 13$ to $V \simeq 16.5$, corresponding to a range in stellar mass from $\sim 1.4 M_{\odot}$ ($(B - V)_0 \sim 0.37$) to $\sim 0.7 M_{\odot}$ ($(B - V)_0 \sim 1.1$), with solar mass stars at $V \sim 15$ ($(B - V) \sim 0.58$). Masses are derived using the Yale (Y2) stellar evolution models (Yi et al. 2003). The cluster reddening ($E_{(B-V)} = 0.20$) was adopted from Deliyannis et al. 2004 (in preparation).

All spectroscopic data were obtained using the WIYN¹ 3.5m telescope at Kitt Peak, Arizona, USA. The telescope is equipped with a Multi-Object Spectrograph (MOS) consisting of a fiber optic positioner (Hydra) feeding a bench mounted spectrograph. The Hydra positioner is capable of placing ~ 95 fibers in a 1-degree diameter field with a precision of $0.2''$. In the field of M35 approximately 82-85 fibers are positioned on stars while the remaining fibers are used for measurements of the sky background. We use the $3''$ diameter fibers optimized for blue transmission, and the spectrograph is configured with an echelle grating and an all-transmission optics camera providing high throughput at a resolution of $\sim 20,000$. All observations were done at central wavelengths of 5130\AA or 6385\AA with a wavelength range of $\sim 200\text{\AA}$, providing rich arrays of narrow absorption lines. Radial velocities with a precision of $\sim 0.5 \text{ km s}^{-1}$ (Meibom et al. 2001) are derived from the spectra via cross-correlation with a high S/N sky spectrum.

Telescope time granted from NOAO² and Wisconsin allowed for 3-4 observing runs per

¹The WIYN Observatory is a joint facility of the University of Wisconsin-Madison, Indiana University, Yale University, and the National Optical Astronomy Observatories.

²NOAO is the national center for ground-based nighttime astronomy in the United States and is operated by the Association of Universities for Research in Astronomy (AURA), Inc. under cooperative agreement with the National Science Foundation.

year for M35, with each run typically including multiple observations on several sequential nights. Once identified, velocity variables are observed at a frequency appropriate to the timescale of their variation. At present the radial-velocity survey has resulted in a sample of 81 spectroscopic binaries: 32 members, 37 candidate members and 12 non-members. Of the 32 member binaries, 25 are single-lined (SB1) and 7 are double-lined (SB2) spectroscopic binaries. The orbital periods span from 2.25 days to 1115 days among the member binaries, corresponding to separations from ~ 0.04 to 2.5 AU assuming a $1 M_{\odot}$ primary and a $0.5 M_{\odot}$ secondary component. The 32 member binaries were identified in the 2MASS All Sky Survey based on equatorial coordinates. 2MASS ID's, astrometry, photometry, and orbital parameters are listed in Table 1.

Table 1. Astrometric, photometric and orbital data for binary members of M35.

2MASS ID ¹	MS ID ²	Cd ID ³	α (2000) h m s	δ (2000) ° ' "	V	$B - V$	Binary type	# RV's	γ (kms^{-1})	Period (days)	e	MP (%) ⁴	M_{prim} (M_{\odot})	M_{sec} (M_{\odot})	Spectral type
06090257+2420447	249	402	06 09 02.550	+24 20 44.62	13.62	0.60	SB1	32	-8.3	10.280	0.009 ±0.019	99	1.32	...	F7
06090403+2423483	252	404	06 09 04.010	+24 23 48.26	13.31	0.63	SB2	11/9	-8.7	22.490	0.155 ±0.017	99	1.28	1.01	M
06090521+2419309	259	410	06 09 05.180	+24 19 30.92	13.32	0.60	SB1	25	-8.4	2.703	0.028 ±0.028	99	1.32	...	F7
06090650+2413499	267	419	06 09 06.470	+24 13 49.90	14.62	0.75	SB1	18	-6.8	344.6	0.334 ±0.030	97	1.05	...	G0
06091099+2421515	301	447	06 09 10.960	+24 21 51.51	13.65	0.62	SB1	20	-7.7	58.02	0.502 ±0.029	97	1.28	...	F8
06092037+2412177	360	512	06 09 20.340	+24 12 17.74	13.64	0.62	SB2	15/7	-8.5	35.380	0.272 ±0.017	99	1.28	0.83	M
06093861+2417394	463	612	06 09 38.590	+24 17 39.54	14.38	0.73	SB1	18	-8.1	79.28	0.375 ±0.010	94	1.05	...	G0
06083426+2421359	06 08 34.220	+24 21 35.73	16.03	1.16	SB2	18/7	-7.9	56.14	0.353 ±0.026	...	0.77	0.77	M
06085047+2419382	06 08 50.440	+24 19 38.16	16.42	1.26	SB2	19/14	-5.3	24.108	0.219 ±0.013	...	0.69	0.66	M
06090352+2417234	06 09 03.490	+24 17 23.36	15.95	1.10	SB1	18	-7.5	156.9	0.594 ±0.024	...	0.77	...	K1
06091557+2410422	06 09 15.540	+24 10 42.16	15.47	1.03	SB1	36	-7.9	8.170	0.538 ±0.013	...	0.77	...	K1
06091924+2417223	06 09 19.210	+24 17 22.37	15.53	0.92	SB1	18	-8.8	795	0.208 ±0.045	...	0.86	...	G7
06092436+2426200	06 09 24.330	+24 26 20.03	15.34	0.88	SB1	22	-7.4	10.330	0.016 ±0.009	...	0.95	...	G3
06084130+2426389	06 08 41.260	+24 26 38.88	16.10	1.14	SB1	18	-6.9	18.426	0.276 ±0.016	...	0.77	...	K1
06090444+2412441	06 09 04.410	+24 12 44.00	14.86	0.80	SB1	15	-9.1	49.075	0.358 ±0.018	...	0.95	∞...	G3
06093267+2415041	06 09 32.640	+24 15 04.14	14.26	0.67	SB1	12	-7.46	7.088	0.003 ±0.005	...	1.19	...	F9
06104368+2416089	06 10 43.680	+24 16 09.05	14.50	0.82	SB1	17	-9.5	10.077	0.008 ±0.005	72	0.95	...	G3
06101134+2426415	06 10 11.350	+24 26 41.42	15.32	1.02	SB1	32	-6.4	14.524	0.246 ±0.044	...	0.86	...	G7
06095563+2417454	06 09 55.627	+24 17 45.60	15.02	0.88	SB1	18	-7.5	30.130	0.273 ±0.005	...	0.95	...	G3
06094745+2423085	494	650	06 09 47.455	+24 23 08.56	13.63	0.67	SB1	15	-6.9	1114.97	0.543 ±0.072	90	1.19	...	F9
06092221+2446528	06 09 22.217	+24 46 52.68	15.00	0.78	SB1	15	-8.6	8.010	0.041 ±0.032	72	0.95	...	G3
06092708+2413452	404	550	06 09 27.094	+24 13 45.12	13.80	0.73	SB2	20/15	-10.2	4.442	0.010 ±0.006	98	1.05	0.92	M
06092536+2404037	...	541	06 09 25.363	+24 04 03.72	13.76	0.61	SB2	24/20	-7.5	16.488	0.041 ±0.014	57	1.28	1.13	M
06085334+2432309	198	343	06 08 53.335	+24 32 30.80	14.32	0.67	SB1	15	-8.0	22.619	0.404 ±0.007	96	1.19	...	F9
06085441+2403081	06 08 54.418	+24 03 08.06	14.97	0.77	SB1	19	-7.45	12.280	0.550 ±0.003	...	1.05	...	G0
06083296+2408164	06 08 32.969	+24 08 16.30	15.05	0.78	SB1	17	-7.3	457.0	0.512 ±0.064	...	0.95	...	G3
06083082+2417547	06 08 30.818	+24 17 54.67	15.47	0.88	SB2	16/15	-10.3	18.590	0.429 ±0.009	...	0.95	0.89	M
06083184+2410384	75	229	06 08 31.841	+24 10 38.35	14.57	0.74	SB1	18	-7.1	475	0.507 ±0.021	89	1.05	...	G0
06080751+2423413	9	122	06 08 07.500	+24 23 41.46	13.94	0.60	SB1	19	-8.3	930	0.474 ±0.079	98	1.32	...	F7
06074436+2430262	06 07 44.352	+24 30 26.10	15.23	0.82	SB1	11	-6.9	473	0.309 ±0.121	...	0.95	...	G3
06100456+2437000	06 10 04.562	+24 37 00.19	15.74	1.03	SB1	16	-8.3	12.566	0.095 ±0.006	...	0.86	...	G7
06083789+2431455	06 08 37.889	+24 31 45.48	15.95	1.05	SB1	14	-8.1	2.247	0.010 ±0.008	...	0.77	...	K1

ferences. — (1) 2MASS ID's; (2) McNamara & Sekiguchi (1986) ID's; (3) Cudworth (1971) ID's; (4) Proper motion membership probability by McNamara & Sekiguchi (1986); Cudworth (1971)

3. THE PERIOD-ECCENTRICITY DISTRIBUTION IN M35

The new compilation of binary orbits in M35 greatly improves the constraint on tidal circularization at the early stage of the main-sequence phase. Prior to this publication, the small sample of binary orbits in the Pleiades provided only rough limits on the transition between eccentric and circular orbits at this age (Mermilliod et al. 1992). Figure 1 shows the distribution of orbital eccentricity (e) as a function of \log orbital period (P) for the 32 spectroscopic binary members of M35. The shortest period binaries have orbital eccentricities consistent with circular orbits, while the orbits for longer period binaries show a distribution of non-zero eccentricities. The presumably primordial distribution of eccentricities for the longest period binaries is consistent with the Gaussian distribution observed in late-type main-sequence binary populations in other open clusters (Duquennoy et al. 1992), in the solar neighborhood (Duquennoy & Mayor 1991), and from the Galactic halo (Latham et al. 2002). The lack of high eccentricity orbits ($e \gtrsim 0.6$) among the long period binaries in M35 may be due in part to observational biases.

All binaries whose periods and eccentricities are plotted in Figure 1 are cluster members based on their radial velocities and location in the color-magnitude diagram (CMD). Fifteen have confirmation of membership from proper-motion measurements. A few binary systems deserve special attention and Figure 2 shows on a linear scale the distribution of orbital eccentricity vs. period for binaries with periods less than 20 days. The last 4 digits of the 2MASS ID are used to label key binaries in Figure 2 and for reference in the text and in Table 1. Nine binary orbits have eccentricities less than $3 \times \sigma_e$ above $e = 0.0$, where σ_e denotes the error on the orbital eccentricity. We consider these binary orbits to be circular. Binary 4037 ($P_{orb} = 16.49$ days, $e = 0.041 \pm 0.014$) has the longest period among the binaries with circular orbits. Three circular binaries have orbital periods close to 10 days: 6089 ($P_{orb} = 10.08$ days, $e = 0.008 \pm 0.005$), 0447 ($P_{orb} = 10.28$ days, $e = 0.009 \pm 0.019$), and 6200 ($P_{orb} = 10.33$ days, $e = 0.016 \pm 0.009$). 4 binaries have eccentric orbits with periods shortward of the longest period circular orbit: 0422 ($P = 8.17$ days, $e = 0.538 \pm 0.013$), 3081 ($P = 12.28$ days, $e = 0.550 \pm 0.003$), 7000 ($P = 12.57$ days, $e = 0.095 \pm 0.006$), and 6415 ($P = 14.52$ days, $e = 0.246 \pm 0.044$).

Thus regardless of the homogeneity in age, metallicity and primary mass of the M35 binary population there is a ~ 8 day overlap in period between eccentric and circular binary orbits.

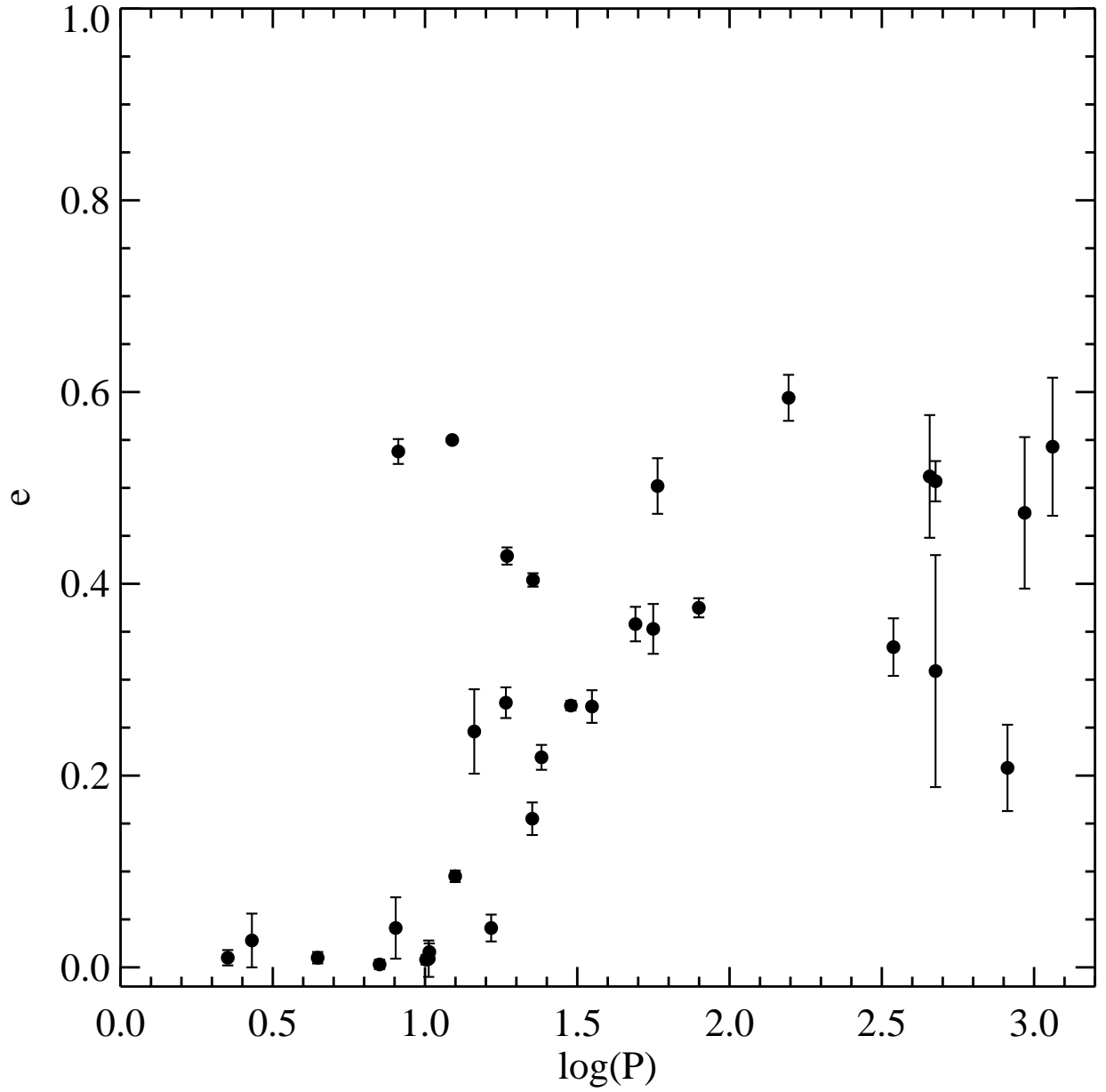


Fig. 1.— The distribution of orbital eccentricity (e) as a function of \log orbital period (P) for 32 solar-type spectroscopic binary members in M35.

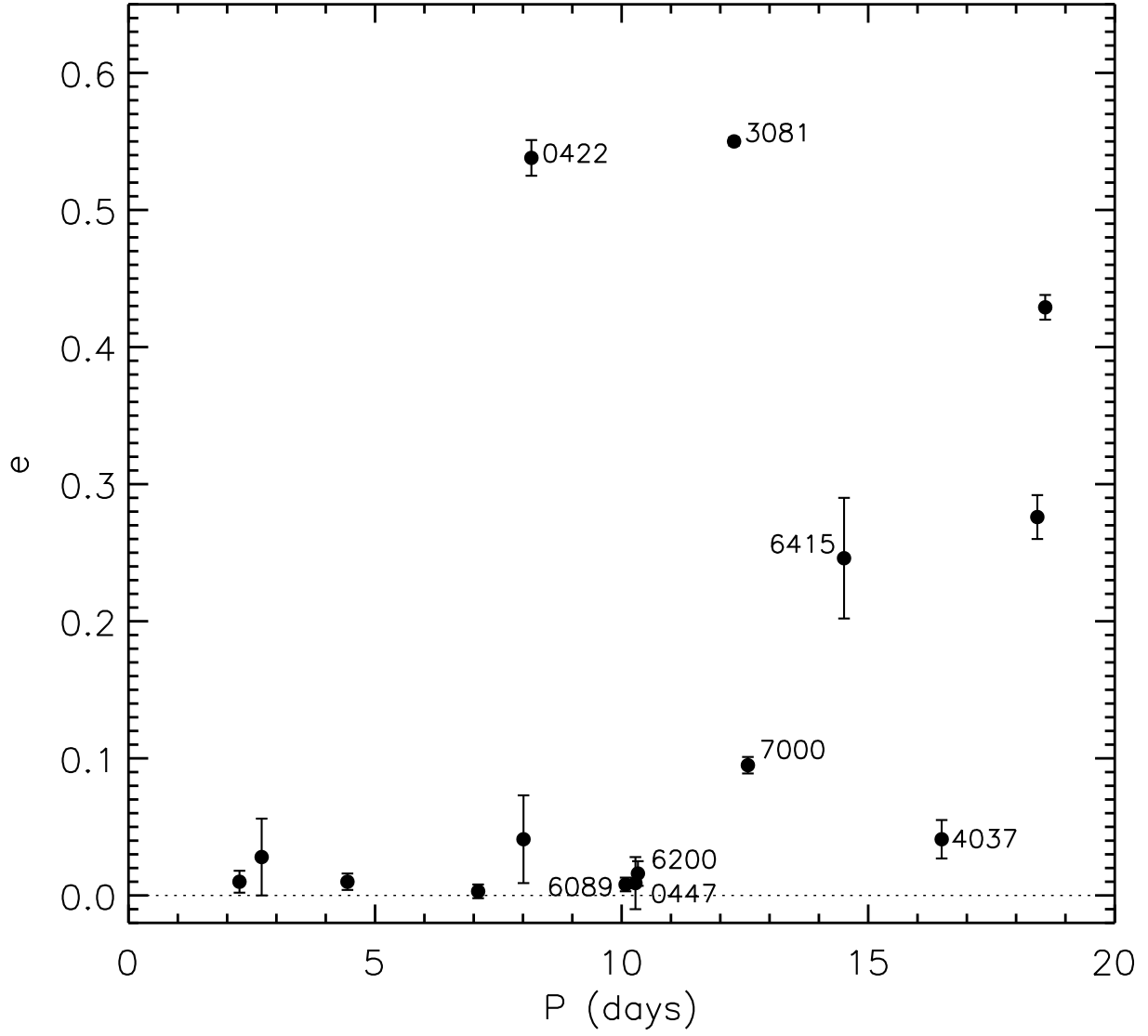


Fig. 2.— The eccentricity distribution of M35 binary orbits with periods shorter than 20 days. Numbers next to selected data refer to binary ID numbers in Table 1.

4. DETERMINING THE CIRCULARIZATION PERIOD

The transition from eccentric to circular orbits observed in M35 is also found in observational studies of late-type main-sequence binary populations in well known open clusters such as the Pleiades (Mermilliod et al. 1992), the Hyades/Praesepe (Duquennoy et al. 1992; Mermilliod & Mayor 1999), M67 (Latham et al. 1992), and NGC188 (Mathieu et al. 2004), and in populations of PMS (Melo et al. 2001, and references therein), field (Duquennoy & Mayor 1991), and halo (Latham et al. 2002) binaries. This characteristic fingerprint of tidal circularization is an important observational constraint on the theory of tidal circularization. Consequently, determination of the period at which binary orbits becomes circular in a given binary population is critical to constraining theoretical models. However, determining this tidal circularization period is not straightforward in any of the above populations.

The longest period circular orbit has been the preferred measure over the past decade (e.g. Duquennoy et al. 1992) and has been referred to as the *tidal circularization cutoff period* (hereinafter: cutoff period). We argue here that the cutoff period is not the optimal measure of the transition between eccentric and circular orbits.

Populations of short period binaries vary in size and consist of systems with a distribution of initial eccentricities. This is observed in the Gaussian distribution of orbital eccentricity at longer orbital periods where presumably orbital evolution has been minimal (Halbwachs et al. 2003; Duquennoy et al. 1992; Duquennoy & Mayor 1991). The Gaussian distribution of initial orbital eccentricities combined with the effects of tidal circularization will lead to an overlap in period-space between initially low eccentricity orbits that have been circularized and initially high eccentricity orbits not yet circularized. This overlap is indeed observed in all published populations of coeval binary orbits with the exception of the small sample in the Pleiades cluster (see Section 7, Figure 8). The width of this overlap was estimated by Mathieu & Mazeh (1988) based on the observed distribution of initial orbital eccentricities, and indeed, Duquennoy et al. (1992) showed that the existence of eccentric orbits in the Hyades/Praesepe populations with periods shorter than the longest period circular orbit can be explained due to incomplete tidal circularization of binaries with initially high orbital eccentricity. We similarly find through simulations of tidal circularization using the equilibrium tide theory by Zahn (1977) that eccentric orbits with periods shorter than the longest period circular orbit can be a result of high initial eccentricity ($e \gtrsim 0.5$).

For short-period binaries with low but non-zero orbital eccentricity ($0.0 \lesssim e \lesssim 0.1$), Mazeh (1990) suggests that the eccentricity is induced by the presence of a third companion star due to dynamical interactions different from tidal effects. However, most eccentric orbits with periods shorter than the longest period circular orbit have eccentricities between 0.1 and 0.6, and among the 4 binaries in M35 with moderate to significant eccentricities and

periods shortward of the longest period circular orbit we see no indications in the stellar spectra of a third component.

Monte Carlo simulations of tidal circularization using the equilibrium tide theory by Zahn (1977) show that the longest period circular binary orbit defining the cutoff period is likely to originate from the low eccentricity tail of the initial Gaussian eccentricity distribution. Accordingly, the cutoff period does not measure tidal circularization of the most frequent binary orbit. We show in Figure 3 the $e - \log(P)$ diagram of a tidally circularized population of artificially generated binaries (grey diamonds). To focus on the process of tidal circularization, the lower limit on the initial orbital eccentricity was set to 0.05 (dotted horizontal line). The threshold of 0.05 is 2-3 times the typical error on orbital eccentricities determined from observations. The initial and final locations of the longest period circular orbit are marked with an open and a filled circle, respectively.

Figure 3 also demonstrate that the probability of measuring the “true” cutoff period of a parent population of binaries is highly sensitive to the size of the observed binary population. Consequently, the value of the observed cutoff period will vary with the size of the population.

Furthermore, long period ($P \sim 2 \times 10^1 - 10^2$ days) circular ($e < 0.05$) or marginally circular ($e \lesssim 0.1$) orbits of unevolved binaries are observed in the majority of the published binary populations (see Section 7, Figure 8), indicating the possibility that binary stars can also form with very low eccentricity. While not included in Figure 3, the cutoff period is vulnerable to such primordial circular orbits.

Finally, the determination of the cutoff period makes no use of the information provided by eccentric orbits in the $e - \log(P)$ diagram.

Consequently we suggest that the cutoff period is not a robust measure of the state of tidal circularization in a coeval binary population.

So motivated, we propose a new method for determining the period of circularization of primordial eccentric binary orbits. We refer to this period as the *tidal circularization period*. Our proposed method will make use of the information provided by all binary orbits in a population by fitting to the observed period-eccentricity distribution a function of the form:

$$e(P) = \begin{cases} 0.0 & \text{if } P \leq P' \\ \alpha(1 - e^{\beta(P'-P)})^\gamma & \text{if } P > P' \end{cases} \quad (1)$$

This mathematical function is motivated by the observed period-eccentricity distributions and by numerical modeling using the theory of Zahn (1977). The function is not

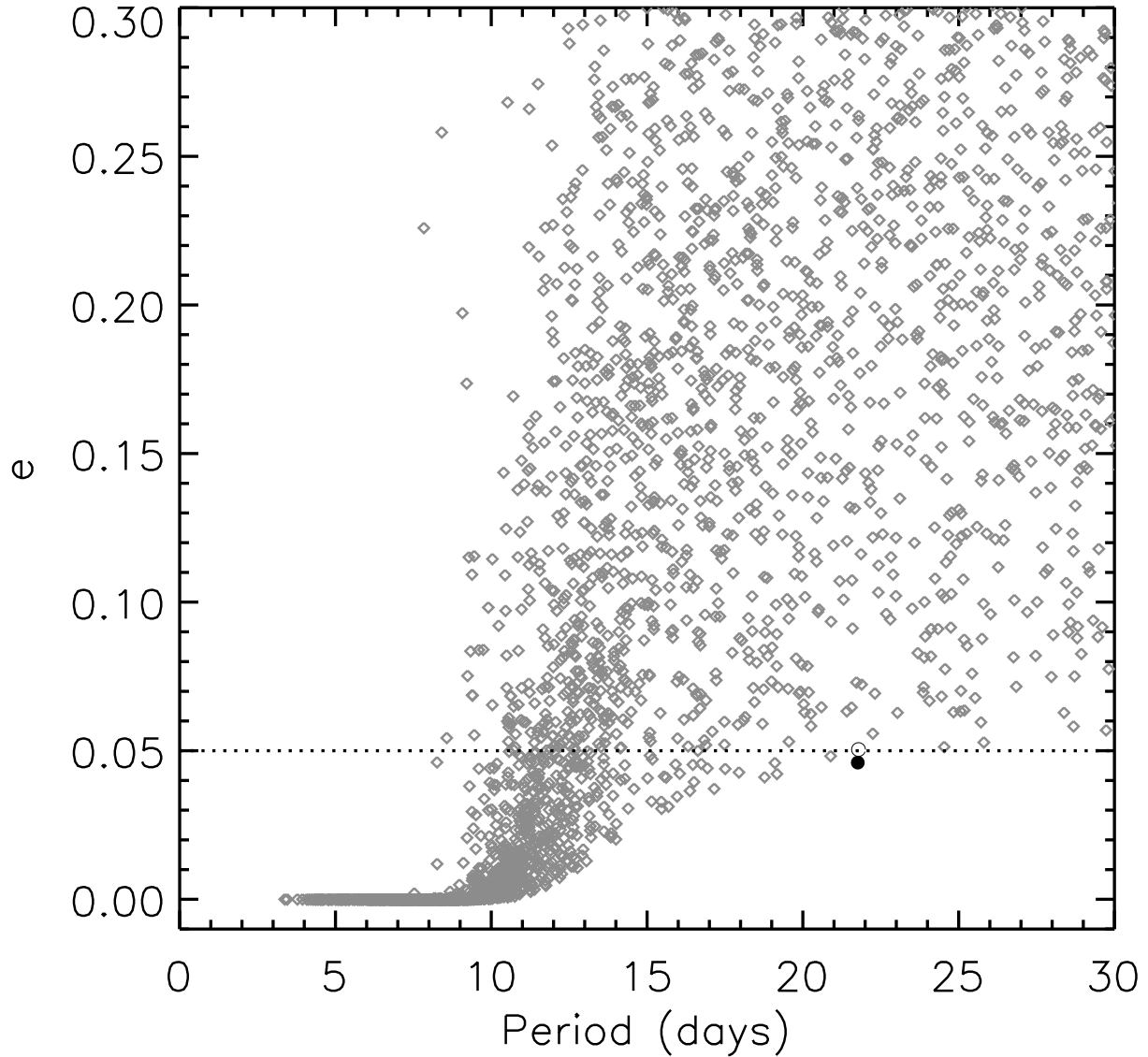


Fig. 3.— The $e - \log(P)$ diagram for a tidally circularized population of artificially generated binaries (grey diamonds). The lower limit on the initial orbital eccentricity is shown as a dotted line at $e = 0.05$. The initial and final locations of the longest period circular orbit are marked with an open and a filled circle, respectively.

physically derived but constructed to mimic the tidal circularization isochrone of the most frequently occurring eccentric binary orbits. Figure 4 shows the function in the $e - \log(P)$ diagram. The transition of the function from eccentric to circular orbits is managed by the $e^{\beta(P'-P)}$ term and the γ coefficient. γ controls the abruptness of the break from $e = 0$ at the period P' and β controls the overall steepness/slope of the transition. Our choices of β and γ are discussed in Section 5. The value of α ($\alpha = 0.35$) is set to ensure that $e(P > P')$ approaches a value of 0.35, the mean eccentricity of all observed binary orbits with periods longer than 50 days in the Pleiades, M35, Hyades/Praesepe, M67, and NGC188. For periods shortward of P' the function is set to 0.0 ($e(P < P') = 0.0$). We will hereafter refer to this function as the circularization function.

The value of P' determines the location of the onset of the rise in the circularization function. We determine the location of the circularization function in period by minimizing the total absolute deviation (δ) between the observed (e_i) and the calculated ($e(P_i)$) eccentricities,

$$\delta = \sum_{i=1}^N | e_i - e(P_i) |^\eta . \quad (2)$$

N denotes the number of binary orbits. The value of the exponent η controls the influence on P' by the binary orbits with maximum deviation from the circularization function. We found that $\eta > 1$ causes high sensitivity to the short period eccentric binaries, often leading to values of P' smaller than the period of the shortest period eccentric orbit. $\eta = 1$ leads to values of P' between the periods of the shortest period eccentric orbit and the longest period circular orbit. We use $\eta = 1$ when fitting the circularization function throughout this paper.

Figure 4 shows the circularization function fitted to an artificially generated sample of binary orbits. Tidal circularization of these binary orbits has been simulated by numerical integration of differential equations derived using equations (4.3) and (4.4) in Zahn (1977) (Note erratum by Zahn (1978)) and the assumptions by Duquennoy et al. (1992):

$$\frac{de}{dt} = \frac{-e}{AP^{16/3}} \quad (3)$$

$$\frac{dP}{dt} = \frac{-3e^2}{AP^{13/3}} \quad (4)$$

The constant A controls the effectiveness of tidal dissipation and thus the rate of tidal circularization. We set A so that numerical simulation of tidal circularization using equations

(3) and (4) produce transitions from eccentric to circular orbits at periods similar to those observed.

The circularization function mimics the transition from eccentric to circular orbits of the “typical” binary ($0.3 < e_{ini} < 0.4$; highlighted in Figure 4). The tidal circularization isochrone for the typical binary is reproduced by the circularization function at $e = 0.01$. Thus we define the “tidal circularization period” (hereinafter circularization period or CP) as the period for which the best fit circularization function has a value of 0.01 ($e(CP) = 0.01$). The choice of $e = 0.01$ as the threshold for circularization is also similar to the threshold chosen in theoretical simulations (see Section 8), and thus facilitates direct comparison between observations and theory.

Our estimate of the initial eccentricity of a binary orbit that circularizes with a period equal to the circularization period at the age of a binary population, is tied to the tidal theory of Zahn (1977). Deviations from the typical (most frequent) initial eccentricity depends on the value of the circularization period (the age of the binary population). By fitting the circularization function to rich distributions of tidally circularized binary orbits (as shown in Figure 4), we find that over the range of circularization periods of interest to this study, ~ 5 days to 15 days, the range of initial eccentricities of the binaries represented by the resulting circularization periods is 0.2-0.5. This range of initial orbital eccentricities is centered on the mean of the observed Gaussian eccentricity distribution ($\bar{e} = 0.35$) and we conclude that according to the Zahn (1977) theory the circularization period represents the orbital period at which a binary orbit with the most frequent initial orbital eccentricity circularizes. The range of initial eccentricities from 0.2 to 0.5 also includes the initial eccentricity used in theoretical predictions of tidal circularization (see Section 8) facilitating direct comparison between these predictions and the observed circularization periods.

5. EVALUATION OF THE PERFORMANCE OF THE TIDAL CIRCULARIZATION PERIOD

In the following we test the performance of the circularization function and compare its performance to the cutoff period. Using a Monte Carlo approach, we generate 10,000 binary populations each with 20 binaries with periods between 10 and 50 days, corresponding to the number of known binary orbits in the M35 sample with orbital periods shorter than 50 days. Tidal circularization was simulated by numerical integration of the Zahn (1977) differential equations (eqs. [3] and [4] above). Initial orbital periods and eccentricities for each population were determined by random selection from a log-normal period distribution

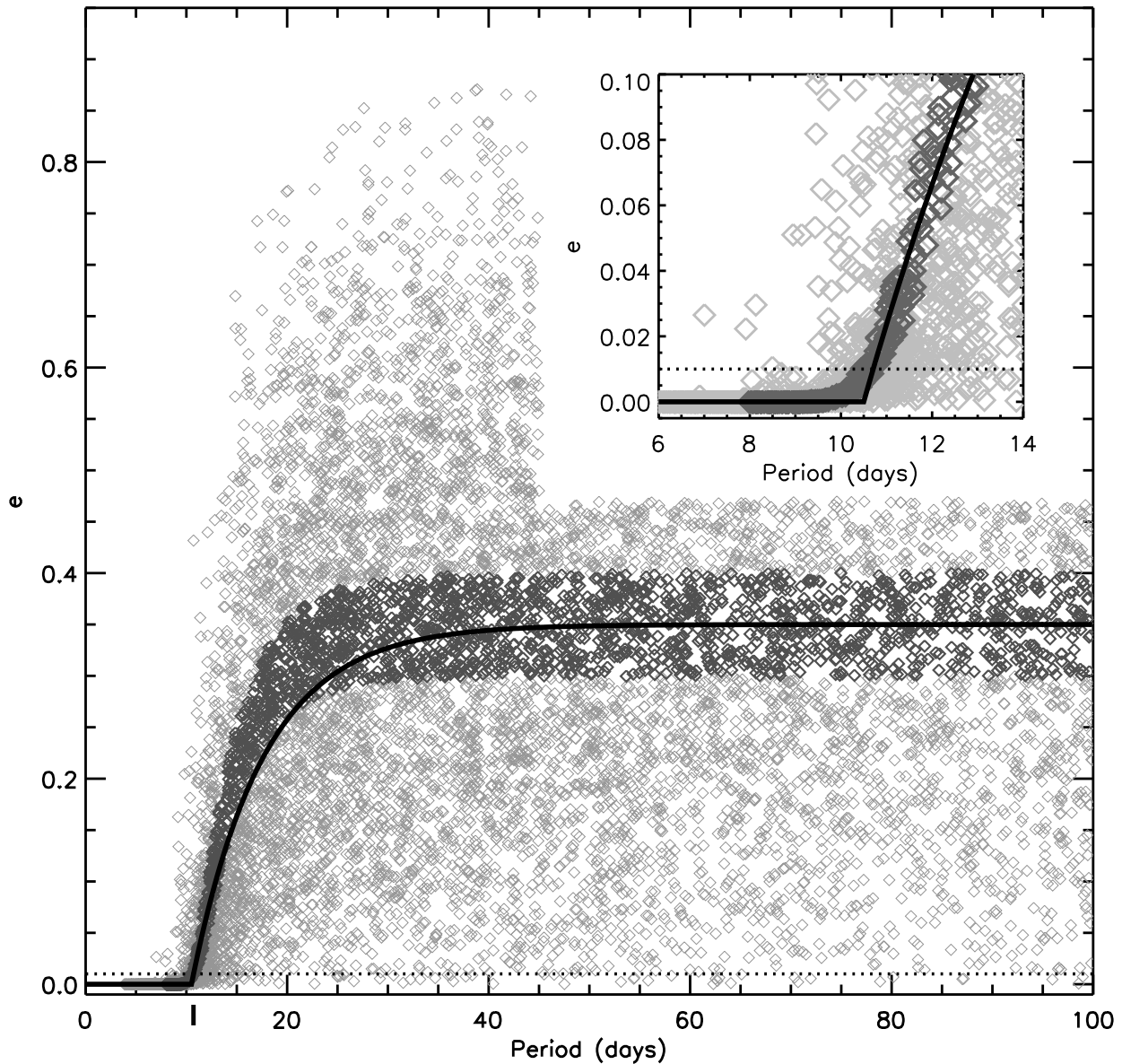


Fig. 4.— The circularization function (black solid line) fitted to an artificially generated sample of binary orbits (diamonds). Tidal circularization of these binary orbits has been simulated by numerical integration of the differential equations (3) and (4). Selection of the initial orbital periods and the initial orbital eccentricities is described in the main text. Binaries with the “typical” (most frequent) initial eccentricities between 0.3 and 0.4 are highlighted (dark diamonds). The circularization period (CP) is defined as the period at which the circularization function has a value of 0.01 ($e(CP) = 0.01$). $e = 0.01$ is marked by a horizontal dotted line and CP is marked by the vertical black line on the period axis. The insert is a close-up view of the transition-region.

and a normal (Gaussian) eccentricity distribution.³ We adopted the period distribution of Duquennoy & Mayor (1991) derived from solar-type binaries in the solar neighborhood, while the Gaussian eccentricity distribution ($\bar{e} = 0.35, \sigma = 0.21$) was determined by fitting the distributions of all orbital eccentricities from the Pleiades, M35, Hyades/Praesepe, M67, and NGC188 for orbits with periods longer than 50 days.

We ran the Monte Carlo experiment twice. The first time we excluded initially circular orbits ($e_i < 0.05$) to test the performance of the diagnostics in the absence of initially circular binaries. The second time we allowed for initially circular orbits to see the effect of such systems on the circularization and cutoff periods.

The distributions of circularization periods and cutoff periods resulting from the two Monte Carlo experiments described above allow us to determine the uncertainty on each of these measures. We will refer to the circularization period and the cutoff period derived from each binary population as the *observed* circularization period and the *observed* cutoff period. For reference two “parent” populations of $\sim 20,000$ binary orbits were generated and tidally evolved. We will refer to the circularization period and the cutoff period derived from these parent populations as the *true* circularization period and the *true* cutoff period.

Figure 5 show the distributions of the observed circularization periods (5a) and the observed cutoff periods (5b) derived for the 10,000 different binary populations *excluding* initially circular binary orbits. The true circularization period is shown in Figure 5a as a vertical solid line at 10.6 days. The distribution of circularization periods is slightly asymmetric with a tail at longer periods. Nonetheless, the true circularization period falls at the mode of the observed distribution. Thus, we take an observed circularization period as the best estimate of the true circularization period for any binary population.

The interval enclosing 2/3 of the observed circularization periods on either side of the mode is marked by dotted vertical lines, and hereafter called the 2/3-interval. We define the uncertainty on the true circularization period of a binary population as the \pm period intervals that the true circularization period can be shifted before the observed circularization period must be drawn from outside of the 2/3-interval. The errorbars on the true circularization period can thus be determined by considering two limiting cases: i) The observed circularization period is located at the short-period boundary of the 2/3 interval; 1.0 days shortward of the mode. In that case the observed circularization period would underestimate the true circularization period by 1.0 days. We assign a positive errorbar of 1.0 days to the true circularization period. ii) The observed circularization period is located at the long period boundary of the 2/3 interval; 1.2 days longward of the mode. In that case the observed

³Orbits randomly selected with an initially negative eccentricity were excluded.

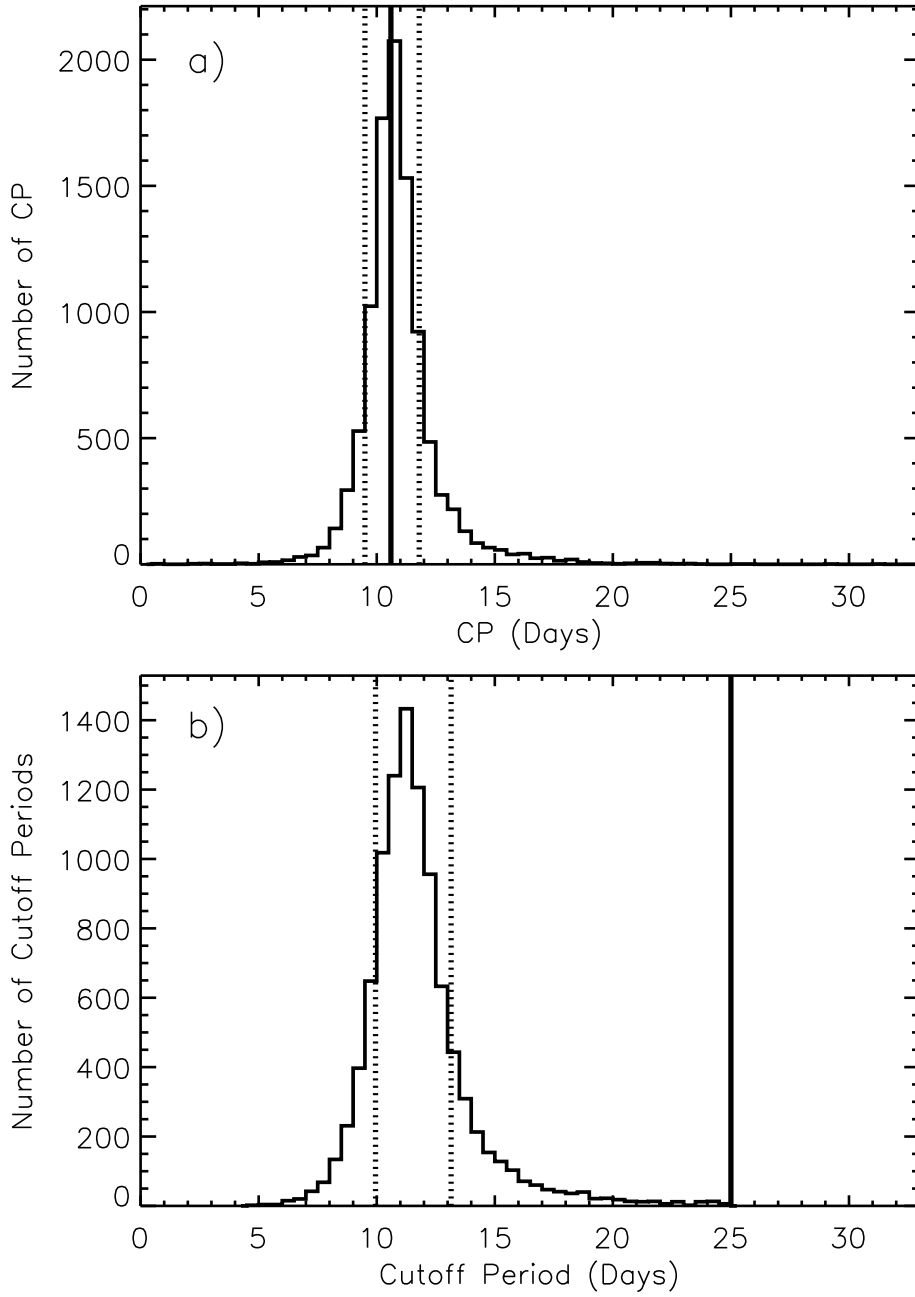


Fig. 5.— **a)** The distribution of circularization periods from 10,000 different binary populations each with 20 binary orbits with periods between 10 and 50 days. Only initially eccentric binary orbits ($e_i > 0.05$) were considered. The vertical solid line mark the location of the true circularization period determined from a “parent” population of $\sim 20,000$ binary orbits (10.6 days). The interval containing 2/3 of all circularization periods around the mode is shown by the two vertical dotted lines at 9.6 and 11.8 days. **b)** The distribution of cutoff periods from the same 10,000 binary populations. The true cutoff period determined from the “parent” population of $\sim 20,000$ binary orbits is marked by a vertical solid line at 25.0 days. The vertical dotted lines at 10.0 and 13.2 days mark the interval containing 2/3 of all cutoff periods around the mode at 11.3 days.

circularization period would overestimate the true circularization period by 1.2 days. We assign a negative errorbar of 1.2 days to the true circularization period.

Accordingly, for a binary sample with ~ 20 orbits shorter than 50 days (e.g. the M35 sample) the uncertainty range around the circularization period is + 1.0 days and - 1.2 days.

The cutoff period of each binary population is defined here as the period of the longest period binary with an eccentricity below 0.05. The distribution of observed cutoff periods in Figure 5b is also slightly asymmetric with a tail toward longer periods and a mode of 11.3 days. The true cutoff period is marked by a vertical solid line at 25 days. Necessarily, the observed cutoff periods are shorter than the true cutoff period, and the mode of the distribution falls 13.7 days shortward thereof.

The measurement uncertainty of the cutoff period is defined similarly to the circularization period. The 2/3-interval is marked by dotted vertical lines, and we define the uncertainty range around our estimate of the true cutoff period as the \pm period intervals that the true cutoff period can be shifted before the observed cutoff period must be drawn from outside of the 2/3-interval. Accordingly, for a binary sample with 20 orbits shorter than 50 days (e.g. the M35 sample) the uncertainty range around the maximum likelihood estimate of the true cutoff period is + 1.3 days and - 1.9 days.

We wish to emphasize that the maximum likelihood observed circularization period and the true circularization period are the same, whereas the maximum likelihood observed cutoff period is offset from the true cutoff period by 13.7 days. The latter difference reflects a significant sample size dependence of the cutoff period that obscures the physical dependence of the age of the binary population.

In addition the Monte Carlo error analysis gives an error on the circularization period that is 1.0 day smaller than the error on the cutoff period. Thus we have shown that the circularization period is both more accurate and more precise than the cutoff period.

Next we consider binary populations *including* initially circular ($e < 0.05$) binary orbits drawn from the Gaussian parent eccentricity distribution. Figure 6 shows the distributions of the observed circularization periods (6a) and the observed cutoff periods (6b) derived for 10,000 binary populations. All vertical lines represent the same quantities as in Figure 5. Note the small effect of initially circular orbits on the distribution of the observed circularization periods and on the true circularization period derived from the parent population. The uncertainty range around the maximum likelihood estimate of the true circularization period is + 1.0 days and - 1.5 days, somewhat inflated by the initially circular orbits.

In contrast, the distribution of cutoff periods is drastically changed by the presence of

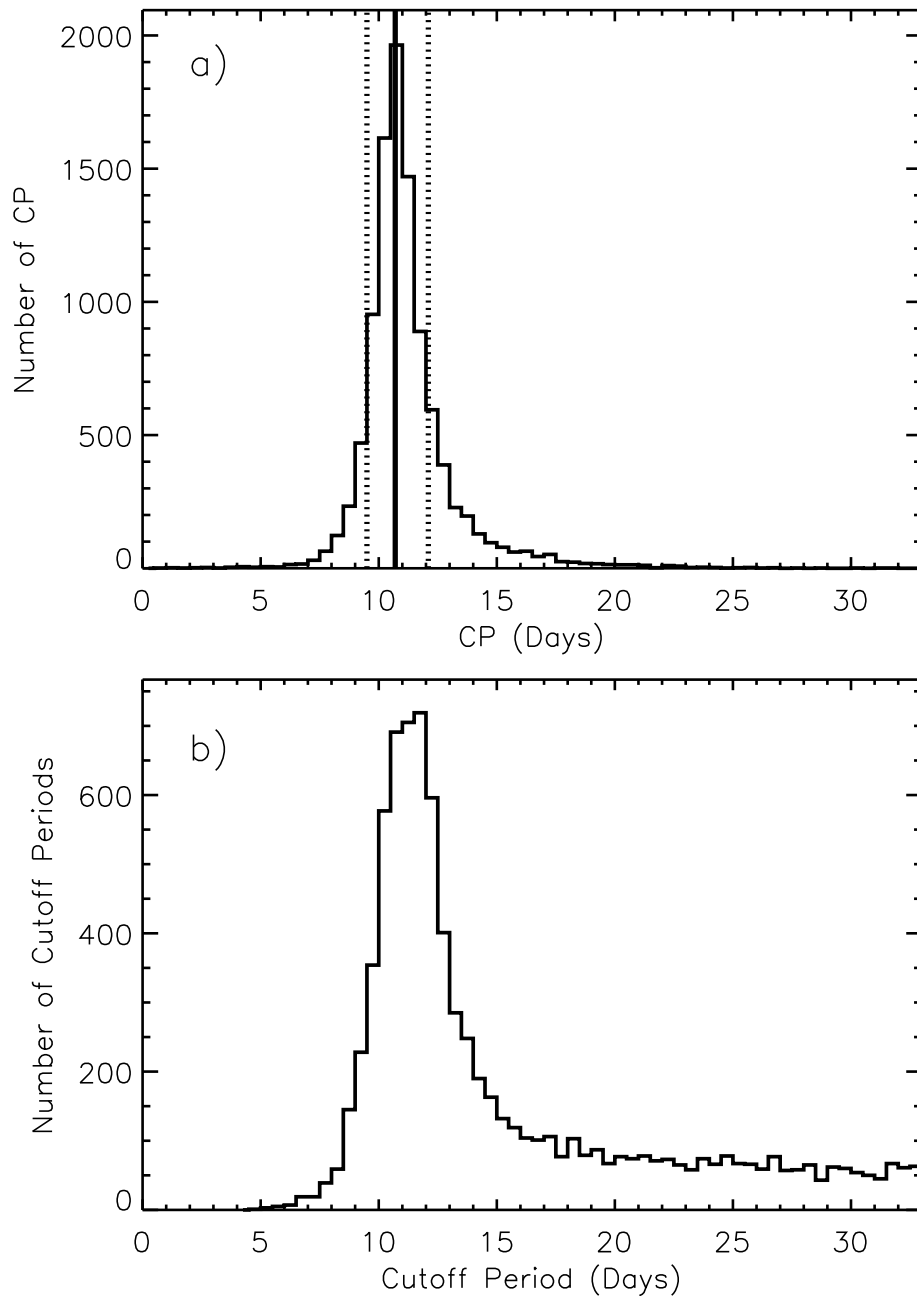


Fig. 6.— **a)** The distribution of circularization periods from 10,000 different binary populations each with 20 binary orbits with periods between 10 and 50 days. Initially circular binary orbits ($e_i < 0.05$) were included. All vertical lines represent the same quantities as in Figure 5. The estimated true circularization period is 10.7 days, and the interval containing 2/3 of all circularization periods around the mode range from 9.7 to 12.2 days. **b)** The distribution of cutoff periods from the same 10,000 binary populations.

initially circular binary orbits ($e < 0.05$). The true cutoff period is undefined and a tail of cutoff periods longward of the distribution mode is produced.

In the presence of binaries with initially low eccentricity determination of the cutoff period is then dependent on the judgment of individual observers to define the eccentricity threshold between circular and eccentric systems and to select the binary defining the cutoff period. Examples of the effect of such judgments/selections on the value of the cutoff period will be given in Section 7 below.

Comparison of Figure 5 and Figure 6 clearly demonstrates the robustness of the circularization period and the vulnerability of the cutoff period. Determination of the circularization period uses the information from all binary orbits, circular as well as eccentric, and is thus less vulnerable to initially circular orbits. The cutoff period is determined from one binary orbit alone and is thus vulnerable to the presence of initially circular orbits in the binary population, contamination from binaries with anomalous evolutionary paths, and/or binaries that have been falsely classified as cluster members.

Importantly, the disadvantages of the cutoff period will be enhanced with larger binary populations, whereas the measurement uncertainty on the circularization period will decrease with increasing population size.

To enable ourselves and colleagues to quote errors on circularization periods to binary populations of different sizes and ages, we repeated the Monte Carlo error analysis (allowing for initially circular binary orbits) 9 times. For each of 3 different sample sizes (10, 20, and 30 binaries) we tidally evolved each of 10,000 samples so that the modes of the circularization period distributions were $\sim 5, 10,$ and 15 days. Errors on the circularization periods were derived in the manner explained above. Table 2 list the derived errors and can be used as a reference for colleagues studying tidal circularization in clusters not listed in this paper.

The coefficients β and γ in the circularization function (eq. [1]) controls the steep-

Table 2. Circularization Period Errors

Size of Binary Population	CP = 5 days Errors (days)	CP = 10 days Errors (days)	CP = 15 days Errors (days)
10 Binaries	+ 1.8 - 1.9	+ 1.5 - 3.1	+ 2.3 - 3.2
20 Binaries	+ 1.2 - 1.2	+ 1.0 - 1.5	+ 1.4 - 2.2
30 Binaries	+ 1.1 - 1.1	+ 0.8 - 1.1	+ 1.2 - 1.5

ness/slope and the abruptness, respectively, of the function’s transition from zero to non-zero eccentricities. Values of 0.14 for β and 1.0 for γ were adopted to minimize the width of the distributions of circularization periods resulting from the Monte Carlo experiments described above, and to minimize the sensitivity of the circularization period to the choice of eccentricity threshold ($e = 0.01$) between circular and eccentric orbits.

6. THE CIRCULARIZATION PERIOD IN M35

After motivating, presenting and testing the circularization function and defining the circularization period, we are ready to apply this new diagnostic of tidal circularization to the population of binary orbits in M35.

Figure 7 show the period-eccentricity distribution in the $e - \log(P)$ diagram of M35. The circularization function resulting in the minimum total absolute deviation between observed and calculated eccentricities is over-plotted and the locations of the observed circularization period (CP) and it’s uncertainty interval are marked. The horizontal dotted line marks $e = 0.01$. The observed circularization period for M35 is $10.2^{+1.0}_{-1.5}$ days. The errors quoted were derived in Section 5 and are listed in Table 2.

The M35 period-eccentricity distribution show striking similarities to the artificially generated distributions created using eqs. (3) and (4) and an initial Gaussian eccentricity distribution. In addition to the period overlap between eccentric and circular orbits described in Section 3, 3 circular binaries with periods of ~ 10 days in M35 nicely represent the most frequent (typical) binaries located in the high density region at $e \lesssim 0.05$ and $P \sim 10$ days in Figure 4. The distribution of eccentricities of binaries with periods longer than ~ 10 days is consistent with a primordial Gaussian distribution and the circular binary (4037) with a period 16.49 days is likely to originate from the low eccentricity wing.

Therefore, M35 is a good example of the advantages of the circularization period in defining the transition between eccentric and circular binary orbits. The best fit circularization function takes advantage of the information provided by all binary orbits and provide a more robust determination of the circularization period for the typical binary orbit.

7. THE CIRCULARIZATION PERIODS OF 7 ADDITIONAL BINARY POPULATIONS

Below we briefly discuss and present the period-eccentricity distributions and determine circularization periods for 7 additional binary populations spanning ages from ~ 3 Myr

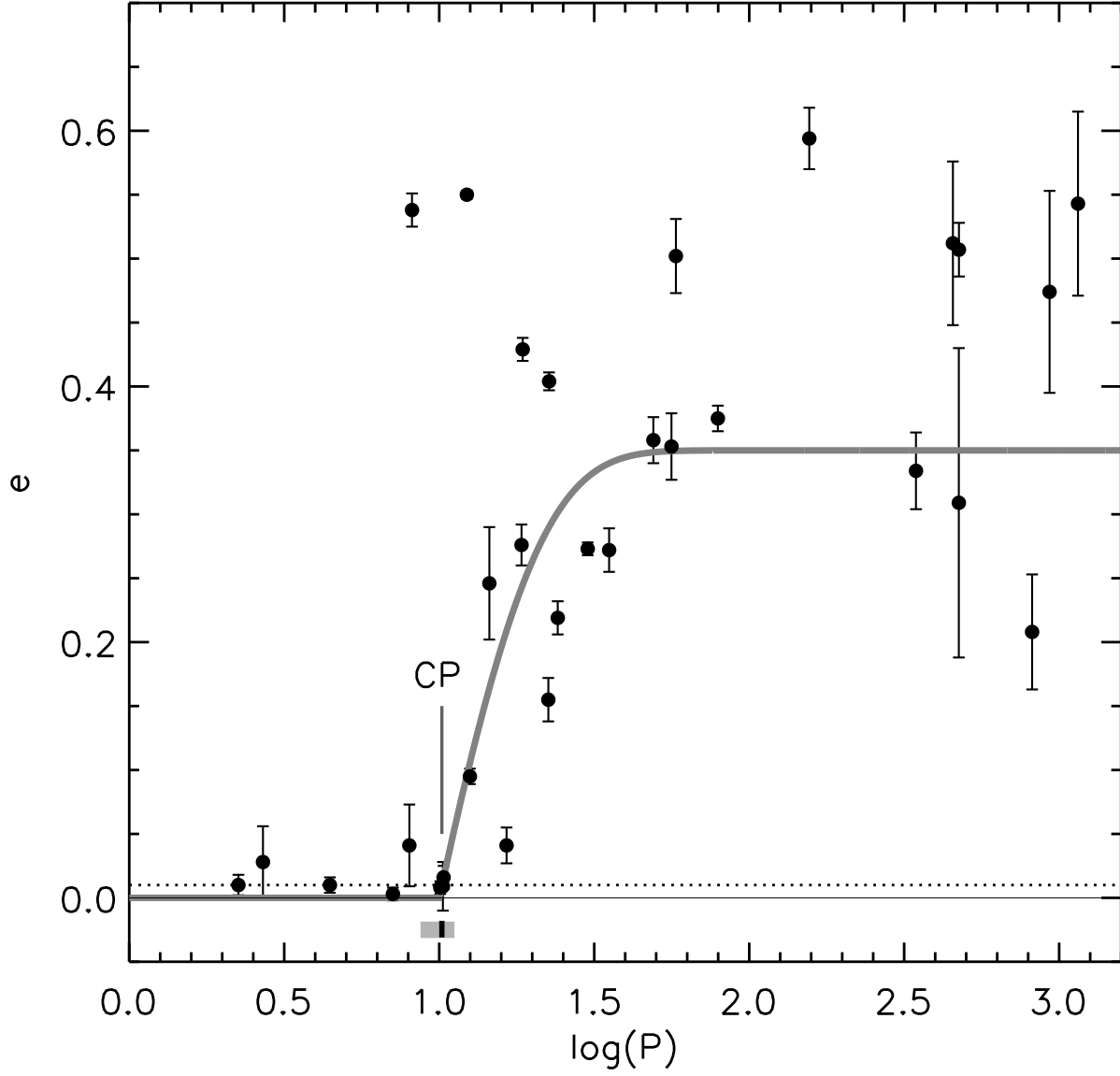


Fig. 7.— The distribution of orbital eccentricity (e) as a function of \log orbital period (P) for 32 spectroscopic binary members of M35. The grey curve represent the best fit circularization function and the dotted horizontal line mark $e = 0.01$. The circularization period (CP) is marked at $\log(P) = 1.0$ (10.2 days) and it's uncertainty interval overlotted.

(PMS binaries) to ~ 10 Gyr (Galactic halo binaries). Figure 8a-h show the orbital data of each individual population with the best-fit circularization function over-plotted and the circularization period with error marked. All results are listed in Table 3; here we briefly discuss each population in turn.

The PMS binary population (Figure 8a): The sample of 37 low-mass PMS binaries show the characteristic period overlap between eccentric and circular orbits. The orbital parameters are taken from Melo et al. (2001), and references to individual binaries can be found in their paper. The PMS sample is not strictly coeval, but cover an age range from ~ 1 -10 Myr (Melo et al. 2001). We determine a circularization period of $7.1_{-1.2}^{+1.2}$ days for the PMS binary sample. This value should be compared to the 7.56 day cutoff period determined by Melo et al. Note, that Melo et al. chose to disregard the circular orbit of binary RX J1301.0-7654a ($P = 12.95$ days ($\log(P) = 1.11$), $e = 0.04 \pm 0.02$; Covino, private communication) based on measurements of super-synchronous rotation of the individual binary components. Because the timescale for tidal synchronization is thought to be shorter than the timescale for circularization (Zahn 1977; Hut 1981), Melo et al. argue that the circular orbit of RX J1301.0-7654a might not be a result of tidal circularization. However, as mentioned by Melo et al., super-synchronous stellar rotation is an expected result of the transition from the PMS to the ZAMS due to conservation of angular momentum and a decline in the efficiency of tidal breaking as the stars contract. Thus we have chosen to include binary RX J1301.0-7654a. However, due to the robust nature of our new diagnostic, excluding binary RX J1301.0-7654a from the PMS sample causes only a 0.5 day decrease in the circularization period, whereas the longest period circular orbit would decrease by 5.39 days (from 12.95 to 7.56 days).

The Pleiades binary population (Figure 8b): The eccentricity distribution of 12 binary orbits in the ~ 100 Myr Pleiades cluster provides poor sampling of the transition region. Also, unlike any other population included in this study, the Pleiades features a gap between the longest period circular and the shortest period eccentric orbit. By fitting the circularization function we make use of the information provided by the binary orbits on both sides of the gap, and determine a circularization period of $7.2_{-1.9}^{+1.8}$ days. This value should be compared to the 7.7 day cutoff period previously used for the Pleiades cluster. The orbital parameters shown in Figure 8b are taken from Mermilliod et al. (1997, 1992). The estimated masses for the binary primary components falls within $\sim 0.9 M_{\odot} - 1.4 M_{\odot}$.

The M35 binary population (Figure 8c): The distribution of orbital eccentricities in M35 (discussed above) is shown here for the purpose of comparison.

The Hyades/Praesepe binary populations (Figure 8d): The sample of 47 binary orbits in the ~ 630 Myr Hyades/Praesepe twin clusters show 3 eccentric binaries shortward of the longest period circular orbit. The best fit circularization function is over-plotted and the

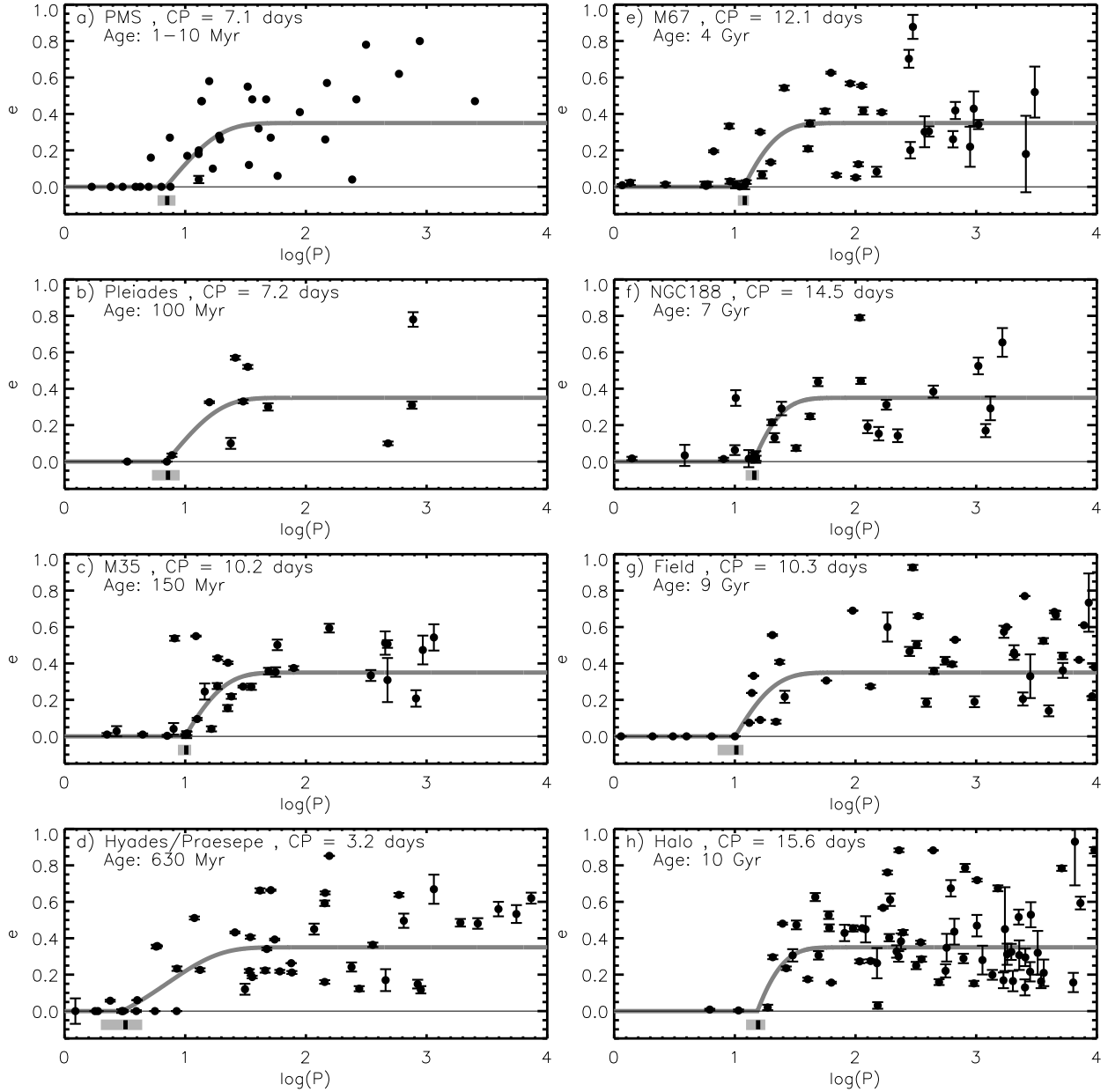


Fig. 8.— The period-eccentricity distributions for 8 late-type binary populations: a) PMS, b) Pleiades, c) M35, d) Hyades/Praesepe, e) M67, f) NGC188, g) field, and h) halo. Overplotted each distribution is the best fit circularization function. A solid horizontal line mark $e(P) = 0.00$. The circularization period (CP) and it’s uncertainty are marked on the period axis by a vertical black line and a grey bar, respectively. The circularization period and the age of the binary population are printed in each plot.

circularization period of $3.2_{-1.2}^{+1.2}$ days is marked. The cutoff period for the Hyades/Praesepe sample has previously been set by the 8.49 day circular binary J331. J331 consist of two $0.5 M_{\odot}$ components, and thus is substantially different from the binaries with approximately solar-mass components defining the transition regions in other binary populations. For this reason Mathieu et al. (1992) questioned whether binary J331 should be disregarded, as the difference in mass and stellar structure (depth of convective envelope) might have significantly altered the timescale of tidal circularization. We will not comment further on the effect of stellar mass here, but simply emphasize that while we have included binary J331, disregarding it leads to no noticeable change in the Hyades/Praesepe circularization period, compared to a -2.75 days change from 8.49 to 5.74 days in the Hyades/Praesepe cutoff period. The orbital parameters shown in Figure 8d are taken from Griffin et al. (1985, 1982); Griffin & Gunn (1981, 1978) for Hyades binaries and Mermilliod & Mayor (1999); Mermilliod et al. (1992, 1990) for Praesepe binaries. The estimated masses for the the primary components of this sample falls within $\sim 0.5 M_{\odot} - 1.5 M_{\odot}$.

The M67 binary populations (Figure 8e): The sample of spectroscopic binaries in the old open clusters M67 contain stellar components ranging in evolution from the unevolved main-sequence to the tip of the giant branch (Mathieu, priv. comm.). As the rate of tidal circularization depends sensitively on stellar radius and the depth of the convection zone, we will consider only binaries in M67 with unevolved primary components. Figure 8e shows the distribution of orbital eccentricity vs. log orbital period for 39 unevolved binaries in M67. Two eccentric orbits are found shortward of the longest period circular orbit. The best fit circularization function is over-plotted and the circularization period of $12.1_{-1.5}^{+1.0}$ days is marked. The mass-range of the binary primary components is $\sim 0.9 M_{\odot} - 1.2 M_{\odot}$.

The NGC188 binary populations (Figure 8f): As for M67, the binary population in NGC188 contains evolved as well as unevolved stellar components. Again we will consider only binaries with unevolved primary components. The distribution of orbital eccentricity vs. log orbital period for 27 unevolved binary stars in NGC188 is shown in Figure 8f. The binary population contains a single eccentric system with a period shorter than the longest period circular binary. The circularization period of $14.5_{-2.2}^{+1.4}$ days is marked and the best fit circularization function is over-plotted. The orbital data shown in Figure 8f are taken from Mathieu et al. (2004). The mass-range of the primary components in this sample is $\sim 0.95 M_{\odot} - 1.05 M_{\odot}$.

The field binary population (Figure 8g): The orbital characteristics of 50 close solar-type binaries from the solar neighborhood (hereinafter: the field) is shown with the circularization period of $10.3_{-3.1}^{+1.5}$ days marked and the best fit circularization function over-plotted. The orbital data are taken from Duquennoy & Mayor (1991), who adopt an age range of 7-11 Gyr

for the population of field binaries. We adopt 9 Gyr as the age of the field sample. However, the age of some individual binary systems are poorly known, thus despite the well-defined circularization period, the age-ambiguities of this sample makes it less reliable for probing the evolution of tidal circularization.

The Galactic halo binary population (Figure 8h): The orbital characteristics of 61 binaries from the Galactic halo. The best fit circularization function is over-plotted and the circularization period of $15.6_{-3.2}^{+2.3}$ days is marked. The orbital data are taken from Latham et al. (2002). We adopt an age of 10 Gyr for the halo binary population. From a large sample of 171 high proper motion spectroscopic binaries, Latham et al. (2002) find no obvious differences between the binary characteristics in the halo and in the disk populations. The observed frequency is the same and the period distributions are consistent with the hypothesis that the binaries are drawn from the same parent population. Nonetheless, the halo binary population is not strictly coeval and the stars differ significantly in mass and metallicity from those of the open cluster/disk populations. Arguably, comparison of solar-mass/solar-metallicity tidal circularization theory to the halo cutoff period requires consideration of these differences.

It is important to note that in the majority of the binary populations discussed here, circular or marginally circular binary orbits are observed with periods from tens to hundreds of days longer than the circularization period. The selection of unevolved main-sequence binaries for each population suggest that these long period ($P \sim 10^1 - 10^2$ days) low eccentricity ($e \sim 0.05$) orbits are not a result of accelerated tidal circularization due to evolved primary components. The existence of long-period low eccentricity binaries in the PMS, Pleiades and M35 samples is a strong indication that binary stars can form with circular or marginally circular orbits, consistent with an initial Gaussian distribution of orbital eccentricities.

The binary populations shown in Figure 8 also show a high frequency of high-eccentricity orbits at periods shorter than the one or more circular orbits. The ability to reproduce such systems from binaries in the high-eccentricity tail of the initial Gaussian distribution by numerically integrating current theoretical models of tidal circularization (Duquennoy et al. 1992, Section 5 this paper), provide further support for the existence of an initial Gaussian distribution of orbital eccentricities.

8. EVOLUTION OF TIDAL CIRCULARIZATION

While different tidal circularization theories agree that the timescale of circularization depends strongly on stellar separation, and that consequently a transition from eccentric

to circular orbits is expected at a well-defined binary period, the different theories describe different mechanisms for the tidal dissipation leading to circularization. The mechanism and efficiency of tidal dissipation in a given model reflects itself in the model’s prediction of the rate of circularization and the evolution of the tidal circularization period. Observational determinations of the circularization periods in binary populations of different ages provide a critical test of the dissipation mechanism(s) responsible.

Detailed discussion of the distribution of circularization cutoff periods with age, and its ability to constrain tidal circularization theory, was given by Witte & Savonije (2002), Melo et al. (2001), and Mathieu et al. (1992). However, the addition of the new large binary populations of M35 and NGC188 (Mathieu et al. 2004), the introduction of a new robust measure of tidal circularization (the circularization period) with measured uncertainties, and the recent theoretical work on dynamical tides in late-type stars (e.g. Witte & Savonije 2002), motivate a fresh look at how the theory compares to the observations.

We show in Figure 9 the circularization periods for all binary populations discussed in this paper (solid/open circles) at their respective ages. Errorbars show the uncertainties on the circularization periods based on the Monte Carlo experiments described in Section 5.

With the exception of the Hyades/Praesepe population, the circularization periods of the coeval solar-type binary populations show a steady increase with age from the PMS and early main-sequence to the late main-sequence phase. The circularization period of the halo and field binaries follow this trend. However, due to the non-coevality and uncertainty in age of the field sample, and the differences in mass and metallicity of the stars in the halo sample, we choose not to include their circularization periods in the subsequent analysis.

The small value of the circularization period of the Hyades/Praesepe sample can be explained in part by the high number of short period eccentric binaries, in particular the two highly eccentric short period binaries (Hyades: HD30738, $P = 5.75$ days, $e = 0.354$; Praesepe: KW181, $P = 5.87$ days, $e = 0.357$). However, even in the absence of these two systems the Hyades/Praesepe circularization period will be 5.9 days and thus still deviate from the overall trend of increasing circularization periods with increasing age. We note that Duquennoy & Mayor (1991) draw attention to an excess of short period binaries ($\log(P) < 1$ day) in the Hyades period distribution when compared to distribution from their G-dwarf sample.

The predictions of main-sequence tidal circularization in the framework of both the equilibrium tide theory and the dynamical tide theory are also shown in Figure 9, as is the prediction by Zahn & Bouchet (1989) including PMS tidal circularization. Note that these different theoretical predictions displayed in Figure 9 use different criteria for determination

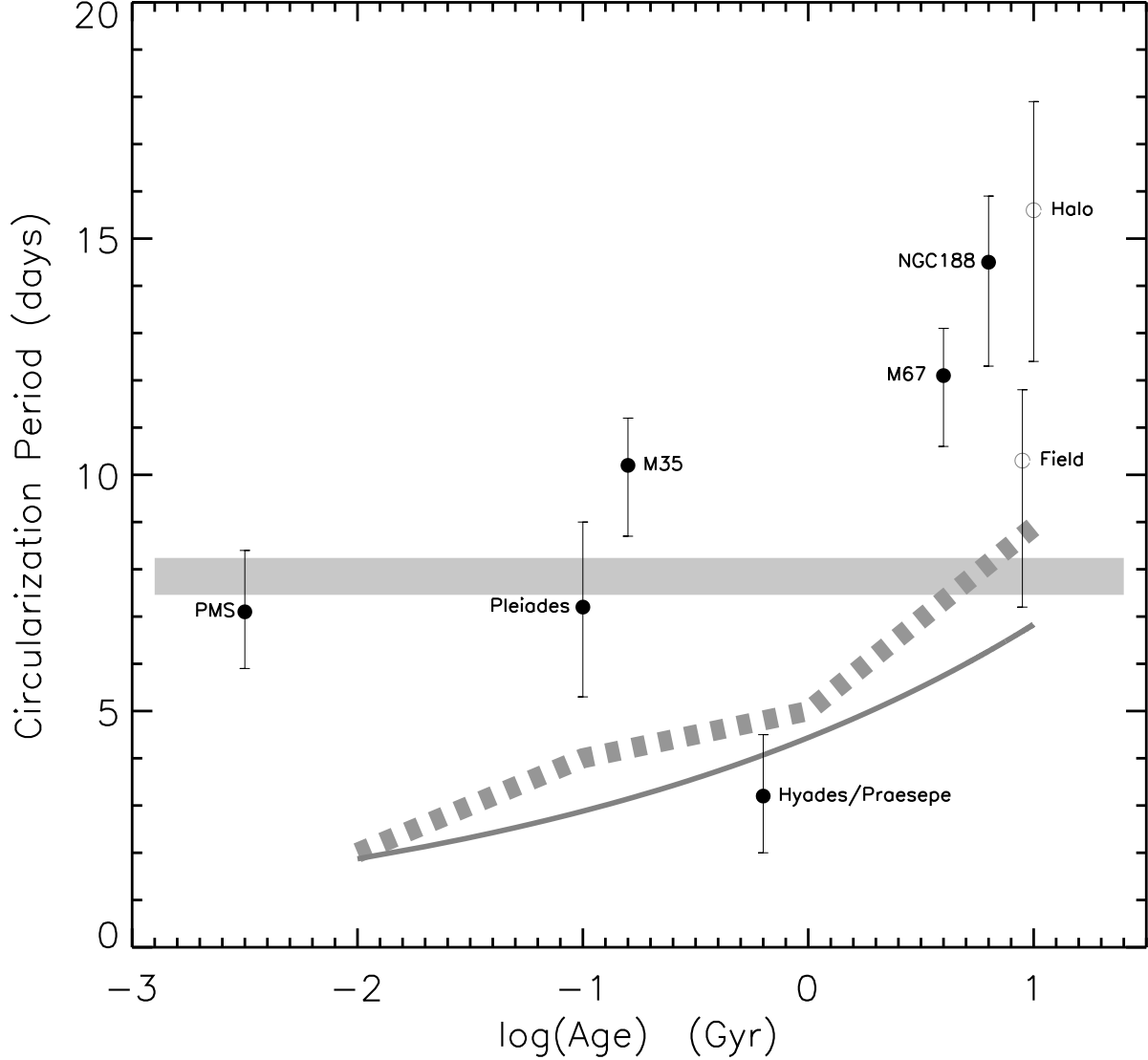


Fig. 9.— The distribution of circularization periods with age for 8 late-type binary population (solid/open circles). Errorbars represent the uncertainties on the circularization periods derived in Section 5. The solid curve shows the predicted cutoff period as a function of time based on main-sequence tidal circularization using the revised equilibrium tide theory by Zahn (1989) (Claret & Cunha 1997). The broad dashed band represent the predicted cutoff period for initially super-synchronous $1 M_{\odot}$ stars calculated in the framework of the dynamical tide model including resonance locking (Witte & Savonije 2002). The horizontal grey band represents the prediction by Zahn & Bouchet (1989) in which tidal circularization is significant only during the PMS phase.

of the cutoff period. Claret & Cunha (1997, equilibrium tide theory) define the cutoff period at a given age as the longest orbital period for which the relative variation in the eccentricity is 0.5% of the initial value ($e_{ini} = 0.30$). Witte & Savonije (2002, dynamical tide theory) define the cutoff period as the longest orbital period for which a binary with $1 M_{\odot}$ components has been circularized to $e < 0.01$. As such the predictions of Witte & Savonije are upper limits on the circularization period. Zahn & Bouchet (1989, PMS tidal theory) define the cutoff period as the period at which a binary with component masses between $0.5 M_{\odot} - 1.25 M_{\odot}$ and initial orbital eccentricity of 0.2 or 0.3 circularizes to $e < 0.005$. Recall that the circularization periods displayed in Figure 9 represent the orbital period at which a binary orbit with initial eccentricities in the range 0.2 - 0.5 evolves to $e = 0.01$ at the age of the population.

The equilibrium tide theory: Let us consider first the equilibrium tide theory using the dissipation mechanism by Zahn (1989). The equilibrium tide theory predicts active tidal circularization throughout the main-sequence phase, leading to longer cutoff periods with increasing population age (solid curve in Figure 9). However, as pointed out by Claret & Cunha (1997), an artificial enhancement of the turbulent dissipation is necessary to fit the observed cutoff periods. Comparison with the new circularization periods, again with the exception of the circularization period of the Hyades/Praesepe population, show a similar discrepancy between the observations and the theoretical predictions of pure main-sequence tidal circularization.

The grey horizontal band in Figure 9 shows the prediction by Zahn & Bouchet (1989) of tidal circularization including the PMS phase. Based on the reduced rate of tidal circularization derived by Zahn (1989), Zahn & Bouchet suggested that all tidal circularization occurs during the PMS phase when the stars have larger radii and deeper convective envelopes. They found that for main-sequence stars the efficiency of turbulent dissipation derived from the equilibrium tide theory is so small that tidal circularization following the PMS phase is negligible despite the Gyr timescales available. Their PMS tidal circularization theory predicts a range of cutoff periods between $\sim 7.2 - 8.5$ days for binaries with components with masses between $0.5 - 1.25 M_{\odot}$ and initial eccentricities of either 0.2 or 0.3. Accordingly, all late-type main-sequence binaries should have circular orbits for period less than ~ 8 days and (primordial) eccentric orbits at longer periods, independent of age.

The hypothesis that PMS tidal circularization alone sets a tidal cutoff period, independent of age, is *not* consistent with the observed distribution of circularization periods. We performed a χ^2 test fitting different constant theoretical circularization periods to the distribution of observed circularization periods. We find that there is less than a 1% probability that the observed circularization periods (excluding or including the field and halo

samples) derive from a model predicting no evolution of the circularization periods with age. Repeating the χ^2 test for all binary populations but the Hyades/Praesepe population also tells us that there is less than 1% chance that the PMS, Pleiades, M35, M67, and NGC188 populations derive from a model predicting pure PMS circularization.

The dynamical tide theory: The predicted evolution of main-sequence tidal circularization using the dynamical tide theory with inclusion of resonance locking (Witte & Savonije 2002) is shown in Figure 9 as a broad dashed band. The width of the dashed band represents the range of predicted evolutions of the cutoff period for binaries with stellar components rotating at super-synchronous ($\Omega = 2\omega_p$), pseudo-synchronous ($\Omega = \omega_p$), and orbital ($\Omega = \omega$) speeds. Ω , ω_p , and ω denote the initial stellar angular velocity, the orbital angular velocity at periastron, and the average orbital angular velocity, respectively. The masses of the binary components used by Witte & Savonije are $1 M_\odot$.

Regardless of stellar rotation velocity, the dynamical tide theory with inclusion of the resonance locking mechanism (Witte & Savonije 2002) appears to predict slightly more efficient tidal circularization than the equilibrium tide theory throughout the main-sequence phase. However, Witte & Savonije (2002) define the cutoff period as the longest orbital period for which a binary has been circularized to $e < 0.01$. This definition implies that the predicted cutoff periods are likely set by binaries with low initial orbital eccentricities, and thus are not directly comparable to the predictions by Claret & Cunha (1997). Still there is a discrepancy between the predicted level of circularization and the distribution of observed circularization periods. For the special case of very slowly rotating stars, the calculations of Witte & Savonije (2002, not shown in Figure 9) offer a near match to the circularization periods of Pleiades, M35, M67 and NGC188. However, the required stellar rotation periods are of order 100 days for stars in close binary systems with ages between 0.1 and 10 Gyr. Such very slow rotations would be unexpected and thus needs to be observationally established.

The slopes of the main-sequence tidal circularization models match the increase in circularization period seen in Figure 9. Thus if the efficiency of tidal dissipation were to be artificially enhanced for both the equilibrium tide and the dynamical tide theories, the predicted main-sequence evolution for both theories would be in agreement with the observed increase in circularization period for all populations but the Hyades/Praesepe.

The hybrid scenario: The lack of success of both PMS and main-sequence tidal circularization theories to account for the observations of tidal circularization motivated the suggestion of a “hybrid scenario” (Mathieu et al. 1992). The hybrid scenario is heuristic and was motivated by a distribution of cutoff periods that appeared age-independent for populations younger than ~ 1 Gyr while showing a positive correlation with age for populations older than ~ 1 Gyr. The hybrid scenario suggest that tidal circularization in binary

populations younger than ~ 1 Gyr derive from PMS tidal circularization, and that after the passage of ~ 1 Gyr the integrated main-sequence tidal circularization begins to circularize binaries with orbital periods of ~ 10 days.

Considering the new distribution of circularization periods the need for a hybrid scenario is uncertain. With the exception of the Hyades/Praesepe population the observed circularization periods increase with age from the PMS and throughout the main-sequence phase. A χ^2 test shows that there is less than 1% probability that the circularization periods for populations younger than ~ 1 Gyr derive from a model predicting no main-sequence tidal circularization. Excluding the Hyades/Praesepe sample result in χ^2 value of ~ 1 . Thus, the current distribution of circularization periods for the youngest binary populations cannot distinguish between a model predicting an age-independent circularization period or a model predicting a continuous increase in the circularization period from the PMS onward.

If tidal circularization is in fact active throughout the main-sequence phase, the question remains which if any of the suggested dissipation mechanisms is responsible. Either the equilibrium or the dynamical tide mechanisms, or perhaps both in combination, could be responsible for the circularization of binary orbits during the main-sequence phase. However, unless both mechanisms are at work simultaneously, more efficient tidal dissipation is needed in both the equilibrium and the dynamical tide theories. We note that PMS tidal circularization is still needed to explain the 7.1 day circularization period of the PMS sample, and that an increase in the efficiency of turbulent dissipation of the equilibrium tide theory presumably will affect circularization during the PMS as well.

Alternatively, assuming pure PMS tidal circularization, the differences in circularization periods among the binary populations in Figure 9 could be due to differences in initial stellar and circumstellar conditions. Goodman & Dickson (1998) speculate that perhaps the differences in mass and/or metallicity between the younger disk binaries and the older disk and halo binaries could be the cause of differences in cutoff periods set during the PMS phase. While the ranges of primary stellar masses and metallicities of the populations included in this study are similar, other stellar/circumstellar and binary/circumbinary parameters might be of importance to the efficiency and duration of tidal circularization during the PMS phase. The strong dependence of the efficiency of circularization on stellar rotation displayed in the dynamical tide theory by Witte & Savonije (2002) is a powerful example of how differences in initial conditions may affect the evolution of tidal circularization.

It is difficult to draw secure conclusions about the evolution of tidal circularization based on only 6 circularization periods. The future observational goal is to further populate the age vs. circularization period diagram (Figure 9) with reliable circularization periods at carefully selected ages based on large samples of binary orbits from homogeneous coeval

binary populations. Following the present study and the recent publication of binary orbits in NGC188 (Mathieu et al. 2004), we plan to contribute (work in progress) such circularization periods at the ages of the young open cluster M34 (~ 250 Myr) and the intermediate age open cluster NGC6819 (~ 2.5 Gyr). By inspection of Figure 9 it is evident that these future circularization periods will greatly improve the observational constraint on future theoretical models and predictions of tidal circularization in close late-type binary stars.

The future goal for theory of tidal circularization in late-type main-sequence stars is to construct models that combine PMS tidal circularization with main-sequence tidal circularization, and predict more efficient tidal circularization in binaries with main-sequence components to account for the observed evolution of circularization.

9. SUMMARY AND CONCLUSIONS

In a coeval population of binary stars the closest binaries tend to have circular orbits, while wider binaries have orbits with a distribution of non-zero eccentricities. Determination of the orbital period to which binaries have been circularized is an important observational constraint on theoretical models seeking to explain the dissipation mechanism(s) responsible for tidal circularization. Coeval populations of short-period binary orbits are therefore key observational contributions.

However, despite homogeneity in age, mass and metallicity, a population of short-period binaries may be small in size and will consist of systems with a distribution of initial eccentricities. The size of a binary population will affect the uncertainty on its circularization period. The initial eccentricity of a circular binary with a period equal to the circularization period is unknown, but can be estimated through the use of theoretical models. Proper comparison between observed and theoretical circularization periods thus require measurement uncertainties on the observed circularization periods and information about the initial eccentricities of the binaries that circularize at those periods.

The primary contributions of this study are: 1) a new population of solar-type spectroscopic binary orbits for the 150 Myr open cluster M35; 2) a new diagnostic to determine the period of circularization of the most frequently occurring binary; 3) an evaluation of the performance of this new diagnostic providing measurement uncertainties on the resulting circularization periods and information about the initial eccentricity of the binaries that circularize at that period; and 4) a comparison of the distribution of circularization periods from 8 binary populations to the predictions from theoretical models.

The new sample of 32 spectroscopic binary orbits in the “Pleiades age” (~ 150 Myr)

open cluster M35 greatly improves the constraint on tidal circularization at the early stage of the main-sequence phase. Prior to this study, the small sample of binary orbits in the Pleiades provided only very rough limits on the transition between eccentric and circular orbits at this age.

Monte Carlo simulations of tidal circularization using the equilibrium tide theory by Zahn (1977) were used to create artificial $e-\log(P)$ distributions. These simulations, together with the $e-\log(P)$ distributions of M35 and 7 additional published binary populations, were used to critically assess the adequacy of the tidal circularization cutoff period (the period of the longest period circular binary) to measure the degree of tidal circularization. We conclude that the cutoff period is not an optimal measure of the transition between eccentric and circular orbits because of the following disadvantages:

- The simulations of tidal circularization using the equilibrium tide theory by Zahn (1977) show that the cutoff period is likely to originate from the low eccentricity tail of an initial Gaussian eccentricity distribution. Therefore, the cutoff period does not represent the period of circularization of the most frequently occurring binary orbit.
- The expected value of the observed cutoff period of a population of binaries varies with the size of the population.
- The cutoff period is vulnerable to the presence of circular orbits that are not a measure of tidal effects, such as primordial circular binary orbits or orbits of binaries with anomalous evolutionary paths.
- Determination of the cutoff period makes no use of the information provided by eccentric orbits in the $e-\log(P)$ diagram.

Motivated by the need for a more robust determination of the orbital period at which a binary orbit with the most frequent initial orbital eccentricity circularizes, we introduce the circularization function and the circularization period. The functional shape of the circularization function (eq. [1]) is fixed and mimics the transition from eccentric to circular orbits in the $e-\log(P)$ diagram (Figure 4). The circularization period is defined as the period for which the circularization function has a value of 0.01 ($e(CP) = 0.01$). The location in period of the circularization function thus determines the circularization period. The advantages of the circularization function/period are:

- Numerical simulations of tidal circularization using the equilibrium tide theory by Zahn (1977) show that the circularization period is the period at which a binary with the

most frequent initial eccentricity ($e \sim 0.35$) evolves to $e = 0.01$ at the age of the population.

- The circularization period is determined from all binary orbits (circular and eccentric), and so is less vulnerable to primordial circular binaries or binaries with anomalous evolutionary paths.
- The observed circularization period is the best estimate of the true circularization period independent of the size of the binary population.

Monte Carlo error analysis allows us to examine the distribution of the circularization periods. From this analysis we estimate and provide the uncertainty on the circularization period as a function of the size of the binary sample and of the value of the circularization period. We note that even in the absence of initial circular binaries and/or contamination from binaries with anomalous evolutionary paths, the Monte Carlo error analysis show that the uncertainty on the circularization period is smaller than the uncertainty on the cutoff period. Thus we conclude that the circularization period is both more accurate and more precise than the cutoff period.

We present the circularization periods for M35 and 7 additional binary populations ranging in age from ~ 3 Myr to ~ 10 Gyr. With the exception of the circularization period of the Hyades/Praesepe population, the distribution of circularization periods with age show a steady increase from the PMS to the late main-sequence.

We compare the distribution of circularization periods to the predictions by theoretical models. The models of main-sequence tidal circularization using either the equilibrium tide theory (Zahn 1989) or the dynamical tide theory with resonance locking (Witte & Savonije 2002) both predict longer cutoff periods with increasing population age in agreement with the trend in the distribution of circularization periods. **However, the predicted circularization periods fall significantly below the observed circularization periods.** This suggest that the efficiency of the dissipation in these models is too low.

A model including PMS tidal circularization (Zahn & Bouchet 1989) predicts negligible circularization during the main-sequence phase. This prediction is not consistent with the observed distribution of circularization periods.

The need for a hybrid scenario as proposed by (Mathieu et al. 1992) is uncertain. The current distribution of circularization periods for the youngest binary populations cannot distinguish between a model predicting an age-independent circularization period or a model predicting a continuous increase in the circularization period from the PMS onward.

The goal for future theories of tidal circularization in late-type main-sequence binaries is to combine PMS and main-sequence circularization in one model that can account for the circularization periods observed at all ages.

We are very grateful to the referee for thoroughly reading the paper and making suggestions for important improvements. We are thankful to the University of Wisconsin - Madison Astronomy Department, to NOAO, and to the WIYN Telescope Director George Jacoby for the time granted on the WIYN telescope. We would like to express our appreciation for exceptional and friendly support of the WIYN Observatory staff, and to Christopher J. Dolan for designing the datareduction pipeline used to measure stellar radial velocities and for obtaining the first epochs in the dataset presented. We thank Jeff Percival and Charles Corson for developing the infrastructure to make remote observing with the WIYN telescope easy and efficient, Ellen Zweibel for granting us liberal access to the Ariadne supercomputer at UW Madison, and Imants Platais for help with identification of m35 stars in the 2MASS survey. We thank Joel Robbins (UW Mathematics Dept.) and Keivan Stassun for help in the search for the circularization function. This work has been supported by NSF grant AST 97-31302 and by a Ph.D fellowship from the Danish Research Agency (Forskningstyrelsen) to S.M.

REFERENCES

- Claret, A., & Cunha, N. C. S. 1997, *A&A*, 318, 187
- Cudworth, K. M. 1971, *AJ*, 76, 475
- Darwin, G. H. 1879, *The Observatory*, 3, 79
- Duquennoy, A., & Mayor, M. 1991, *A&A*, 248, 485
- Duquennoy, A., Mayor, M., & Mermilliod, J. C. 1992, in *Binaries as Tracers of Stellar Formation. Proceedings of a Workshop held in Bettmeralp, Switzerland, Sept. 1991, in honor of Dr. Roger Griffin*. Editors, Antoine Duquennoy, Michel Mayor; Publisher, Cambridge University Press, Cambridge, England, New York, NY, 1992. LC # QB821 .B55 1991. ISBN # 0521433584. P. 52, 1992, 52
- Giuricin, G., Mardirossian, F., & Mezzetti, M. 1984, *A&A*, 134, 365
- Goodman, J., & Dickson, E. S. 1998, *ApJ*, 507, 938
- Griffin, R. F., Griffin, R. E. M., Gunn, J. E., & Zimmerman, B. A. 1985, *AJ*, 90, 609
- Griffin, R. F., & Gunn, J. E. 1978, *AJ*, 83, 1114
- . 1981, *AJ*, 86, 588
- Griffin, R. F., Mayor, M., & Gunn, J. E. 1982, *A&A*, 106, 221
- Halbwachs, J. L., Mayor, M., Udry, S., & Arenou, F. 2003, *A&A*, 397, 159
- Hut, P. 1981, *A&A*, 99, 126
- Latham, D. W., Mathieu, R. D., Milone, A. A. E., & Davis, R. J. 1992, in *ASP Conf. Ser. 32: IAU Colloq. 135: Complementary Approaches to Double and Multiple Star Research*, 155
- Latham, D. W., Stefanik, R. P., Torres, G., Davis, R. J., Mazeh, T., Carney, B. W., Laird, J. B., & Morse, J. A. 2002, *AJ*, 124, 1144
- Mathieu, R. D., Duquennoy, A., Latham, D. W., Mayor, M., Mermilliod, T., & Mazeh, J. C. 1992, in *Binaries as Tracers of Stellar Formation. Proceedings of a Workshop held in Bettmeralp, Switzerland, Sept. 1991, in honor of Dr. Roger Griffin*. Editors, Antoine Duquennoy, Michel Mayor; Publisher, Cambridge University Press, Cambridge, England, New York, NY, 1992. LC # QB821 .B55 1991. ISBN # 0521433584. P. 278, 1992, 278

- Mathieu, R. D., & Mazeh, T. 1988, *ApJ*, 326, 256
- Mathieu, R. D., Meibom, S., & Dolan, C. J. 2004, *ApJ*, ?
- Matthews, L. D., & Mathieu, R. D. 1992, in *ASP Conf. Ser. 32: IAU Colloq. 135: Complementary Approaches to Double and Multiple Star Research*, 244
- Mazeh, T. 1990, *AJ*, 99, 675
- McNamara, B., & Sekiguchi, K. 1986, *AJ*, 91, 557
- Meibom, S., Barnes, S. A., Dolan, C., & Mathieu, R. D. 2001, in *ASP Conf. Ser. 243: From Darkness to Light: Origin and Evolution of Young Stellar Clusters*, 711
- Melo, C. H. F., Covino, E., Alcalá, J. M., & Torres, G. 2001, *A&A*, 378, 898
- Mermilliod, J.-C., Bratschi, P., & Mayor, M. 1997, *A&A*, 320, 74
- Mermilliod, J. C., & Mayor, M. 1992, in *Binaries as Tracers of Stellar Formation. Proceedings of a Workshop held in Bettmeralp, Switzerland, Sept. 1991, in honor of Dr. Roger Griffin*. Editors, Antoine Duquennoy, Michel Mayor; Publisher, Cambridge University Press, Cambridge, England, New York, NY, 1992. LC # QB821 .B55 1991. ISBN # 0521433584. P. 183, 1992, 183
- Mermilliod, J.-C., & Mayor, M. 1999, *A&A*, 352, 479
- Mermilliod, J.-C., Rosvick, J. M., Duquennoy, A., & Mayor, M. 1992, *A&A*, 265, 513
- Mermilliod, J.-C., Weis, E. W., Duquennoy, A., & Mayor, M. 1990, *A&A*, 235, 114
- North, P., & Zahn, J.-P. 2003, *A&A*, 405, 677
- Pan, K., Tan, H., & Shan, H. 1998, *A&A*, 335, 179
- Rieutord, M. 1992, *A&A*, 259, 581
- Rieutord, M., & Zahn, J. 1997, *ApJ*, 474, 760
- Savonije, G. J., & Papaloizou, J. C. B. 1983, *MNRAS*, 203, 581
- Savonije, G. J., & Witte, M. G. 2002, *A&A*, 386, 211
- Tassoul, J. 1988, *ApJ*, 324, L71
- . 2000, *Stellar rotation (Stellar rotation / Jean-Louis Tassoul. Cambridge ; New York : Cambridge University Press, 2000. (Cambridge astrophysics series ; 36))*

- Tassoul, J.-L., & Tassoul, M. 1996, *Fundamentals of Cosmic Physics*, 16, 337
- Tassoul, M., & Tassoul, J. 1997, *ApJ*, 481, 363
- Terquem, C., Papaloizou, J. C. B., Nelson, R. P., & Lin, D. N. C. 1998, *ApJ*, 502, 788
- Witte, M. G., & Savonije, G. J. 1999a, *A&A*, 341, 842
- . 1999b, *A&A*, 350, 129
- . 2001, *A&A*, 366, 840
- . 2002, *A&A*, 386, 222
- Yi, S. K., Kim, Y., & Demarque, P. 2003, *ApJS*, 144, 259
- Zahn, J.-P. 1970, *A&A*, 4, 452
- . 1975, *A&A*, 41, 329
- . 1977, *A&A*, 57, 383
- . 1978, *A&A*, 67, 162
- . 1989, *A&A*, 220, 112
- Zahn, J.-P., & Bouchet, L. 1989, *A&A*, 223, 112

Table 3. Distribution of Circularization Periods with Population Age

Binary Population	$\log(\text{Age})$ (Gyr)	Circularization Period (days)
PMS Binaries	-2.5	$7.1^{+1.2}_{-1.2}$
Pleiades	-1.0	$7.2^{+1.8}_{-1.9}$
M35	-0.8	$10.2^{+1.0}_{-1.5}$
Hyades/Praesepe	-0.2	$3.2^{+1.2}_{-1.2}$
M67	0.6	$12.1^{+1.0}_{-1.5}$
NGC188	0.8	$14.5^{+1.4}_{-2.2}$
Field Binaries	0.95	$10.3^{+1.5}_{-3.1}$
Halo Binaries	1.00	$15.6^{+2.3}_{-3.2}$